NASA TN D-1640

TECHNICAL NOTE

D-1640

MEASUREMENTS OF FLOW ANGLES IN VICINITY OF TWO LIFTING FOREBODY CONFIGURATIONS AT A MACH NUMBER OF 2.01

By Odell A. Morris and Francis E. McLean

Langley Research Center
Langley Station, Hampton, Va.

NATIONAL AERONAUTICS AND SPACE ADMINISTRATION
WASHINGTON

May 1963

NATIONAL AERONAUTICS AND SPACE ADMINISTRATION

TECHNICAL NOTE D-1640

MEASUREMENTS OF FLOW ANGLES IN VICINITY OF TWO LIFTING FOREBODY CONFIGURATIONS AT A MACH NUMBER OF 2.01

By Odell A. Morris and Francis E. McLean

SUMMARY

An investigation has been conducted in the Langley 4- by 4-foot supersonic pressure tunnel at a Mach number of 2.01 to determine the flow properties in the vicinity of two lifting forebody configurations. Measurements of the downwash and sidewash angles generated by the models were made at angles of attack of about 1°, 3°, and 5° for a range of chordwise, spanwise, and vertical probe positions. Surface pressures were also measured on the models at two chordwise stations for the same angle-of-attack range. Results of the tests showed that large and rapid changes in the measured downwash and sidewash angles occurred for both models with variation in the survey probe position in the region of the model trailing edge.

Comparison of the experimental surface pressures with the theoretical values showed only fair agreement for both model configurations; however, the agreement for model B with the most severe twist and camber shape was good, inasmuch as the designed uniform pressure distribution across the span was obtained.

INTRODUCTION

In a search to find supersonic configurations that provide improved lift and lift-drag ratios, a number of investigations have recently been made at the Langley Research Center on highly swept, twisted, and cambered arrow wings. (For example, see refs. 1 to 3.) These studies indicate that the twisted and cambered wing shows greater promise of improvement than a comparable flat-wing planform; however, the experimental results have failed to reach the full benefits as predicted by linear theory. In order to realize the full theoretical benefits the wing must be twisted and cambered properly to produce optimum loading distribution while avoiding local shocks and separated-flow regions. Also, the effect of the body or forebody on the flow pattern of the wing is important and should be considered in order to obtain the most efficient overall design for a complete configuration.

Therefore, the present investigation was conducted to provide information on the effects of the forebody shape on the flow pattern. The two models used

in this study were designed to represent the forward section of a twisted and cambered arrow wing having a root section of sufficient thickness to simulate a conventional-type body. Measurements of the downwash and sidewash angles in the the vicinity of the models were made at a Mach number of 2.01 for a range of chordwise, spanwise, and vertical probe positions at three angles of attack of the models. Surface pressures were also measured at two chordwise stations on each configuration and compared with linear theory. The results of the investigation are presented herein with a limited analysis.

SYMBOLS

q_∞ free-stream dynamic pressure, lb/sq ft

p_∞ free-stream static pressure, lb/sq ft

p_l local static pressure, lb/sq ft

d diameter, in.

α angle of attack (see fig. 1(c)), deg

β cotangent of Mach angle, $\sqrt{M_\infty^2 - 1}$

$n = \beta \times$ (Cotangent of wing leading-edge sweep angle)

x' chordwise distance from model nose

C_P pressure coefficient, $\frac{p_l - p_\infty}{q_\infty}$

$P_{lift} = C_{P,l} - C_{P,u}$

x,y,z Cartesian coordinates of probe location referenced to models as shown in figure 1(c)

M_∞ free-stream Mach number

M local Mach number

ϵ downwash angularity measured in plane vertical to free-stream direction, positive upward, deg

σ sidewash angularity measured in plane horizontal to free-stream direction, positive inward, deg

Subscripts:

u	upper surface
l	lower surface

MODELS AND APPARATUS

Figure 1 gives the principal dimensions of both models. Model coordinates for two different stations are listed in table I. The configurations, which were designed to represent lifting forebodies, varied mainly in the amount of the model twist and camber. Model A had a relatively flat body with only a small amount of camber and was designed for a lift coefficient of 0.21 with optimum conical load distribution according to the method of reference 4. Model B had considerably more camber than model A and was designed for a lift coefficient of 0.20 with uniform spanwise pressure distribution. The models were constructed of wood and aluminum. They were each instrumented with 40 pressure orifices for measuring upper and lower surface pressures at the two chordwise stations shown in figure 1. The pressure tubes were brought out through the inside of the model sting mount and connected to a multiple manometer board.

Figure 1(c) shows a sketch of the tunnel survey apparatus. The probe actuator provided remotely controlled longitudinal travel of 23 inches. The lateral distance was varied by the permanent tunnel-sting traversing mechanism. The heights of the probe and the angle of attack of the model were manually set for each run. Thus, at a given vertical position, the probe could be placed at any point in the x,y grid pattern. The vertical probe positions investigated are designated as positions 1, 2, and 3 and were located at the body tip level (1), the body midpoint level (2), and the body apex level (3), respectively. (See fig. 1(c).)

Details of the conical tip probe are also shown in figure 1(c). The probe contains four static orifices equally spaced around the 30° cone section and one total-pressure orifice located at the cone nose tip. Each of the five orifices was connected to a separate Statham pressure gage and the data were recorded with an IBM card-punch system.

TESTS, MEASUREMENTS, AND ACCURACIES

The investigation was conducted in the Langley 4- by 4-foot supersonic pressure tunnel at a Mach number of 2.01 and a Reynolds number per foot of 2.5×10^6. Tunnel stagnation pressure was maintained at 10 pounds per square inch with a stagnation temperature of 100° F. The stagnation dewpoint was maintained sufficiently low (-25° or less) so that no condensation effects were encountered in the test section. Pressure measurements on the upper and lower surfaces of the model were recorded from a vertical manometer board.

The downwash and sidewash angles behind the models were investigated for a range of spanwise and chordwise probe positions at three different vertical heights with the models at angles of attack of about 1°, 3°, and 5°. Five pressures were measured at the probe by individual Statham gages having a range of 15 pounds per square inch and an accuracy of 0.1-percent full scale. The outputs of these gages were fed directly to a Brown self-balancing potentiometer and then to an IBM card punch. The computing method of reference 4 was used to determine the flow angles from the five pressures measured at the probe.

The model angle of attack and probe vertical positions were corrected for deflection under load. From a pretest tunnel calibration the accuracies of the probe measurements are estimated to be as follows:

Flow angle, deg	Angularity, deg	x, in.	y, in.	z, in.
0 to 5	±0.20	±0.1	±0.1	±0.20
5 to 10	±.40	±.1	±.1	±.20
10 to 15	±.80	±.1	±.1	±.20
15 to 20	±1.20	±.1	±.1	±.20

RESULTS AND DISCUSSION

Pressure Measurements

The surface pressure measurements obtained in this investigation are presented in figure 2. For both models the magnitude and variation of the pressure coefficients with spanwise distance $\frac{y}{x'}$ were generally similar for both the forward and rearward chordwise positions. The lower surface pressures on each model were generally uniform across the span. The upper surface pressures showed considerably larger spanwise variations on model A than on model B; in fact, the spanwise variation in upper surface pressures on model B was nearly uniform at $\alpha = 0^\circ$.

The data of figure 3 show a comparison of the experimental pressure measurements with theoretical values for both model configurations at zero angle of attack. For model A, sizable differences between the experimental and theoretical values of the lifting coefficients occurred at outboard wing sections $\left(\text{for example, around } \frac{\beta y}{nx'} = 0.6\right)$; these differences were due to the large differences between the theoretical and measured values of the upper surface pressures. For model B (fig. 3(b)), the agreement between the theoretical and experimental lifting pressures was generally good, inasmuch as the designed uniform pressure distribution was obtained across the span; however, the magnitudes of the experimental values were about 25 percent less than the theoretical values.

Flow Measurements

The spanwise variations of the downwash and sidewash measurements are presented in figures 4 and 5. The flow angles are plotted against spanwise distance y for the various chordwise and vertical probe positions tested and for the three model angles of attack. To facilitate comparison of the data for the different probe vertical heights, the data for the three vertical probe positions are replotted on the same origin for three probe chordwise positions in figures 6 and 7.

Both models have large changes in the downwash and sidewash angles with variation in probe position. The variation of the sidewash angle with spanwise distance y appeared somewhat more erratic than the variation of the downwash angles; however, similar trends exist for both parameters at the different angles of attack.

The highest flow angles (both downwash and sidewash) usually occurred near the inboard region at spanwise stations of about 4 to 6 inches with angles as high as about $\pm 20^\circ$ for model A and $\pm 13^\circ$ for model B. However, in most cases, these values decreased rapidly toward the outboard spanwise probe positions. At the forward chordwise position (x = 2 inches), all of the flow angles approach zero values at the extreme outer spanwise stations where the probe tip is in a region of interference-free flow outside of the model Mach cone.

CONCLUDING REMARKS

Measurements have been made in the Langley 4- by 4-foot supersonic pressure tunnel of the sidewash and downwash angles for a range of survey probe positions in the vicinity of two lifting forebody configurations at angles of attack of about 1°, 3°, and 5°. Surface pressures were also measured at two chordwise stations on each configuration and compared with theoretical values. Results of the investigation showed that large and rapid changes in the measured downwash and sidewash angles occurred for both models with variation in the survey probe position in the region of the model trailing edge. Comparison of the experimental surface pressures with the theoretical values showed only fair agreement for both model configurations; however, the agreement for model B with the most severe twist and camber shape was good, inasmuch as the designed uniform pressure distribution across the span was obtained.

Langley Research Center,
National Aeronautics and Space Administration,
Langley Station, Hampton, Va., January 29, 1963.

REFERENCES

1. Carlson, Harry W.: Aerodynamic Characteristics at Mach Number 2.05 of a Series of Highly Swept Arrow Wings Employing Various Degrees of Twist and Camber. NASA TM X-332, 1960.

2. Morris, Odell A., and Robins, A. Warner: Aerodynamic Characteristics at Mach Number 2.01 of an Airplane Configuration Having a Cambered and Twisted Arrow Wing Designed for a Mach Number of 3.0. NASA TM X-115, 1959.

3. Brown, Clinton E., and McLean, Francis E.: The Problem of Obtaining High Lift-Drag Ratios at Supersonic Speeds. Jour. Aero/Space Sci., vol. 26, no. 5, May 1959, pp. 298-302.

4. Tsien, S. H.: The Supersonic Conical Wing of Minimum Drag. Ph. D. Thesis, Cornell Univ., June 1953.

5. Carlson, Harry W.: Measurements of Flow Properties in the Vicinity of Three Wing-Fuselage Combinations at Mach Numbers of 1.61 and 2.01. NASA TM X-64, 1959.

TABLE I.- WING ORDINATES

y, in.	z_u, in.	z_l, in.	y, in.	z_u, in.	z_l, in.
x' = 9.60 in.			x' = 24.00 in.		
Model A					
0	0.933	1.893	0	2.333	4.733
.133	.912	1.825	.333	2.280	4.565
.266	.893	1.760	.666	2.233	4.402
.400	.884	1.700	1.000	2.211	4.250
.533	.888	1.663	1.333	2.221	4.160
.800	.918	1.601	1.999	2.295	4.003
1.066	.966	1.557	2.666	2.417	3.894
1.333	1.040	1.539	3.333	2.602	3.848
1.600	1.117	1.523	4.000	2.794	3.809
1.866	1.181	1.495	4.666	2.954	3.783
2.133	1.217	1.439	5.333	3.044	3.598
2.216	1.222	1.415	5.542	3.056	3.538
2.328	1.231	1.385	5.820	3.078	3.463
2.400	1.233	1.362	6.000	3.083	3.406
2.438	1.229	1.355	6.096	3.099	3.388
2.549	1.252	1.330	6.374	3.132	3.326
2.660	1.283	1.322	6.651	3.208	3.306
2.719	1.325	1.343	6.800	3.312	3.359
2.773	1.384	1.384	6.933	3.460	3.460
Model B					
0	1.000	1.933	0	2.500	4.833
.133	.986	1.872	.333	2.465	4.681
.266	.953	1.793	.666	2.384	4.483
.400	.886	1.679	1.000	2.215	4.198
.533	.786	1.533	1.333	1.967	3.833
.799	.545	1.198	1.999	1.363	2.996
1.066	.461	1.021	2.666	1.153	2.553
1.333	.492	.958	3.333	1.230	2.397
1.600	.572	.946	4.000	1.432	2.365
1.866	.692	.972	4.666	1.730	2.430
2.133	.847	1.034	5.333	2.118	2.585
2.400	1.045	1.138	6.000	2.614	2.847
2.533	1.169	1.214	6.333	2.925	3.035
2.666	1.318	1.318	6.666	3.296	3.296

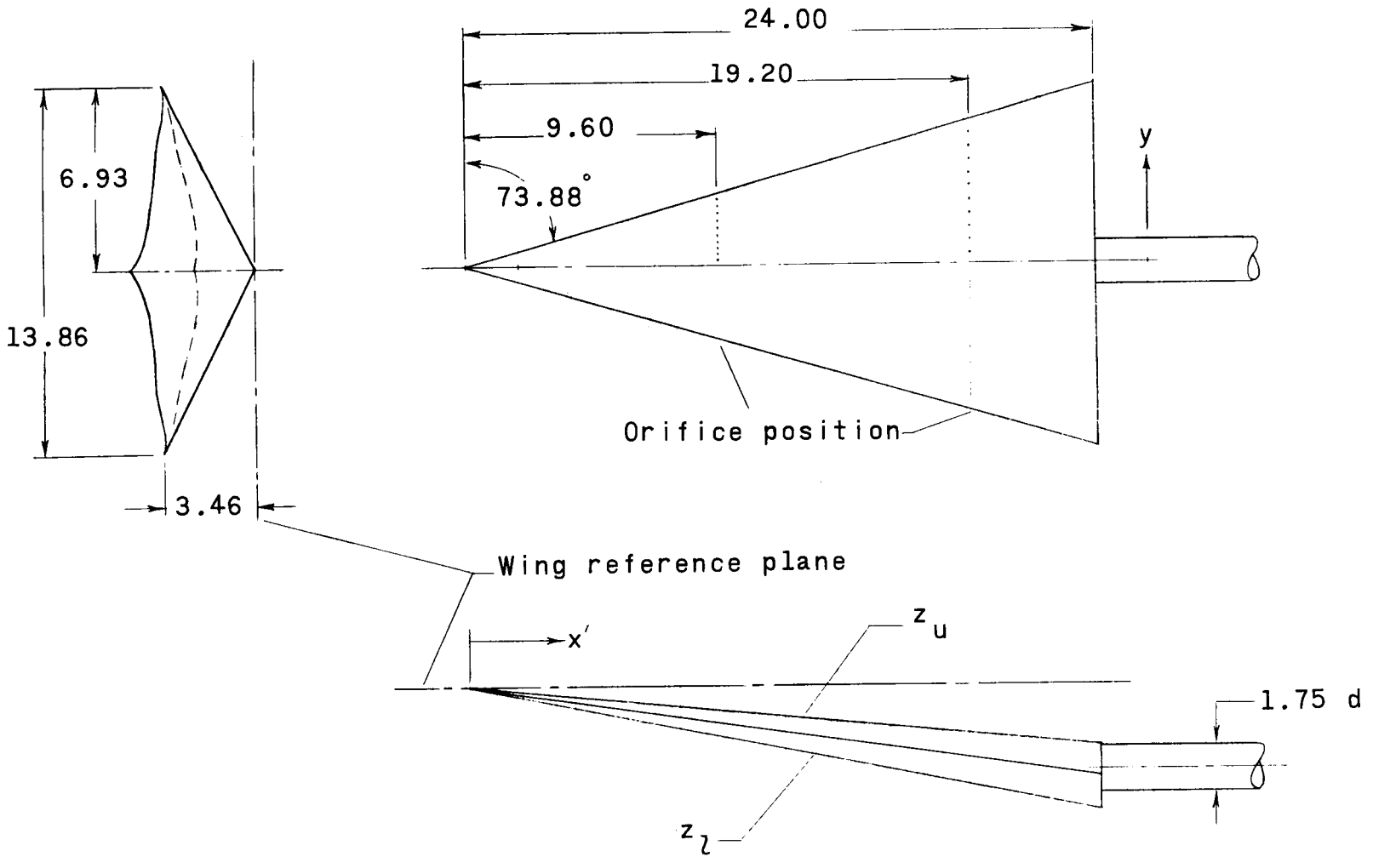

(a) Details of model A.

Figure 1.- Details of models and test setup. (All dimensions are in inches unless otherwise noted.)

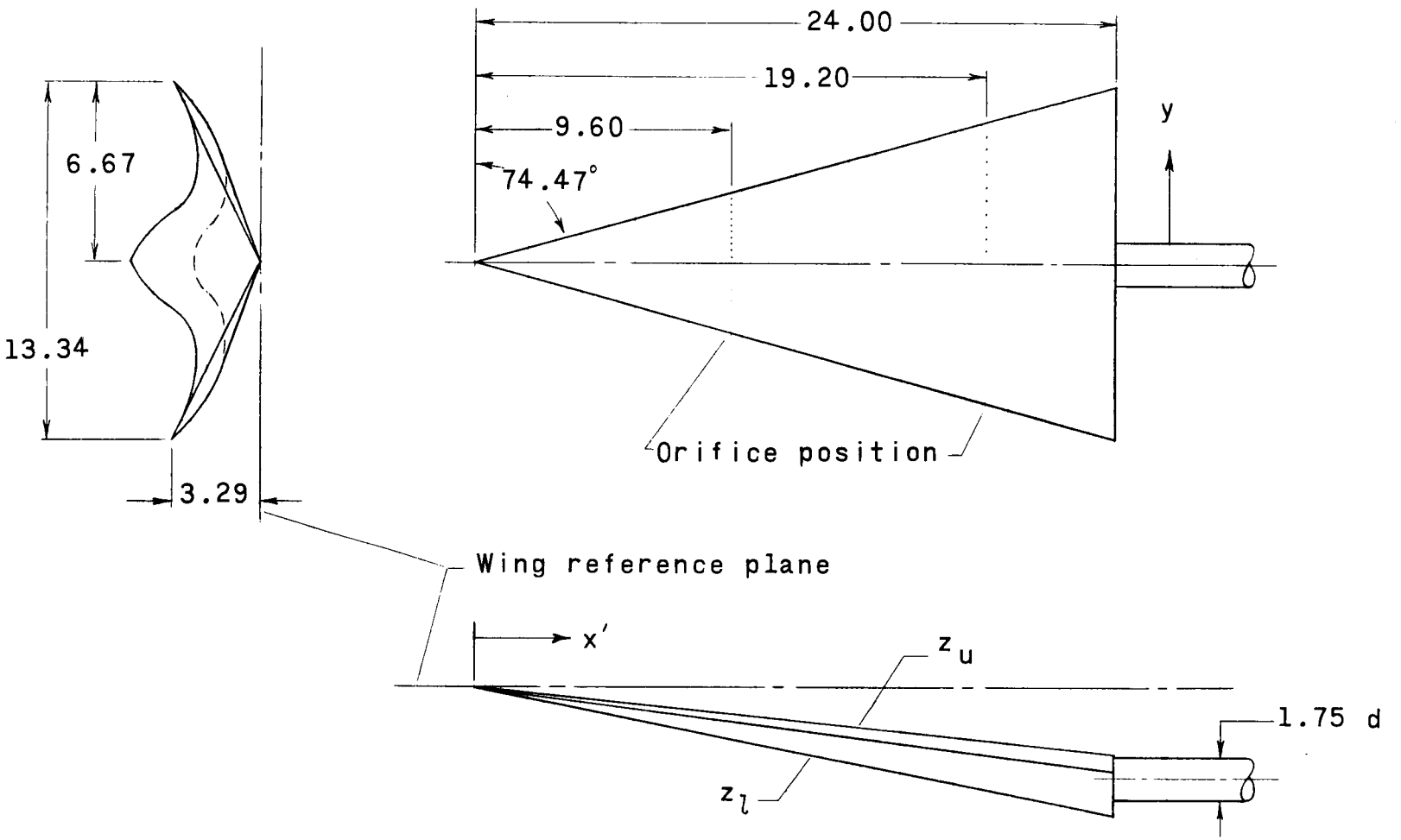

(b) Details of model B.

Figure 1.- Continued.

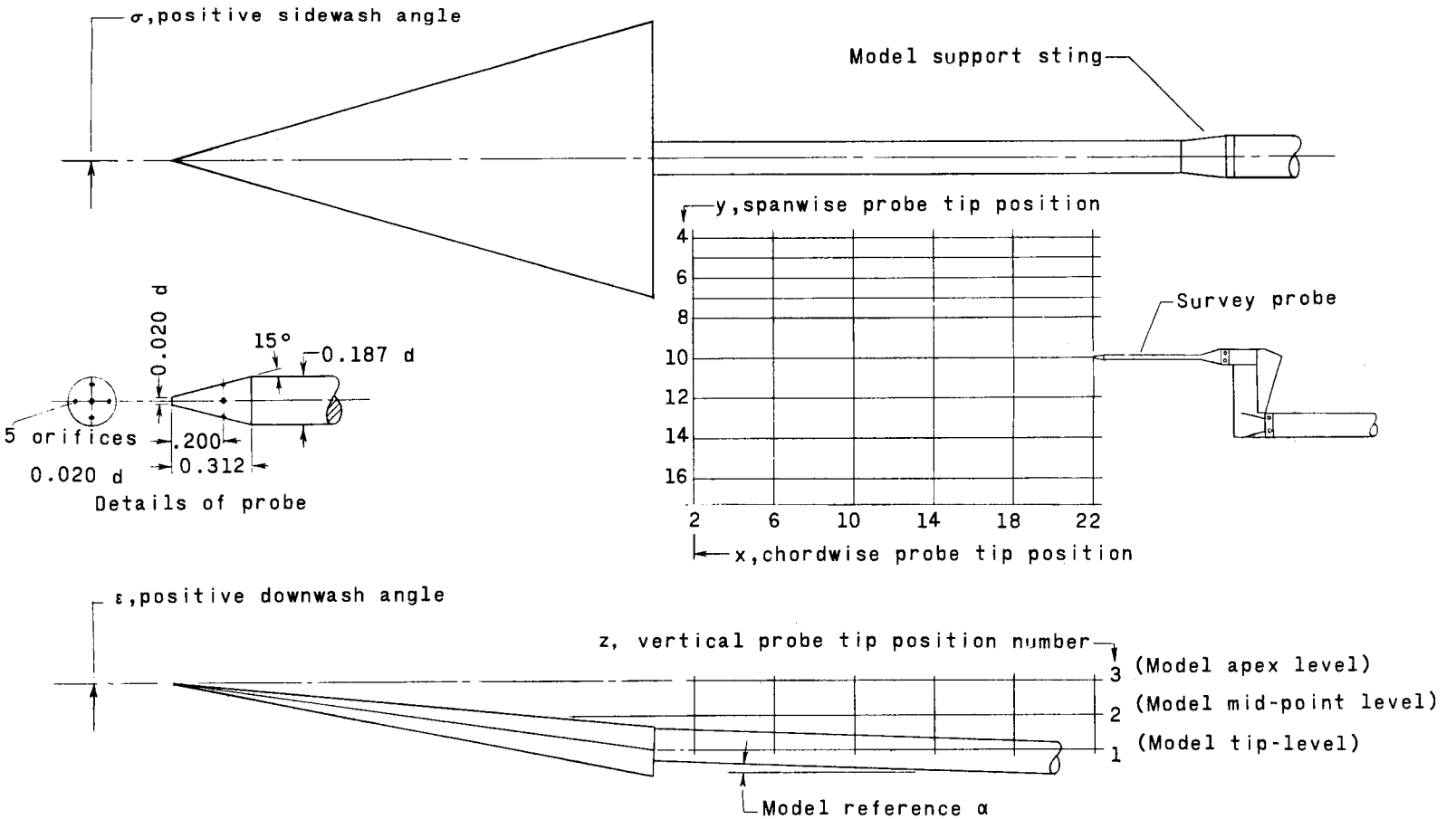

(c) Model test setup.

Figure 1.- Concluded.

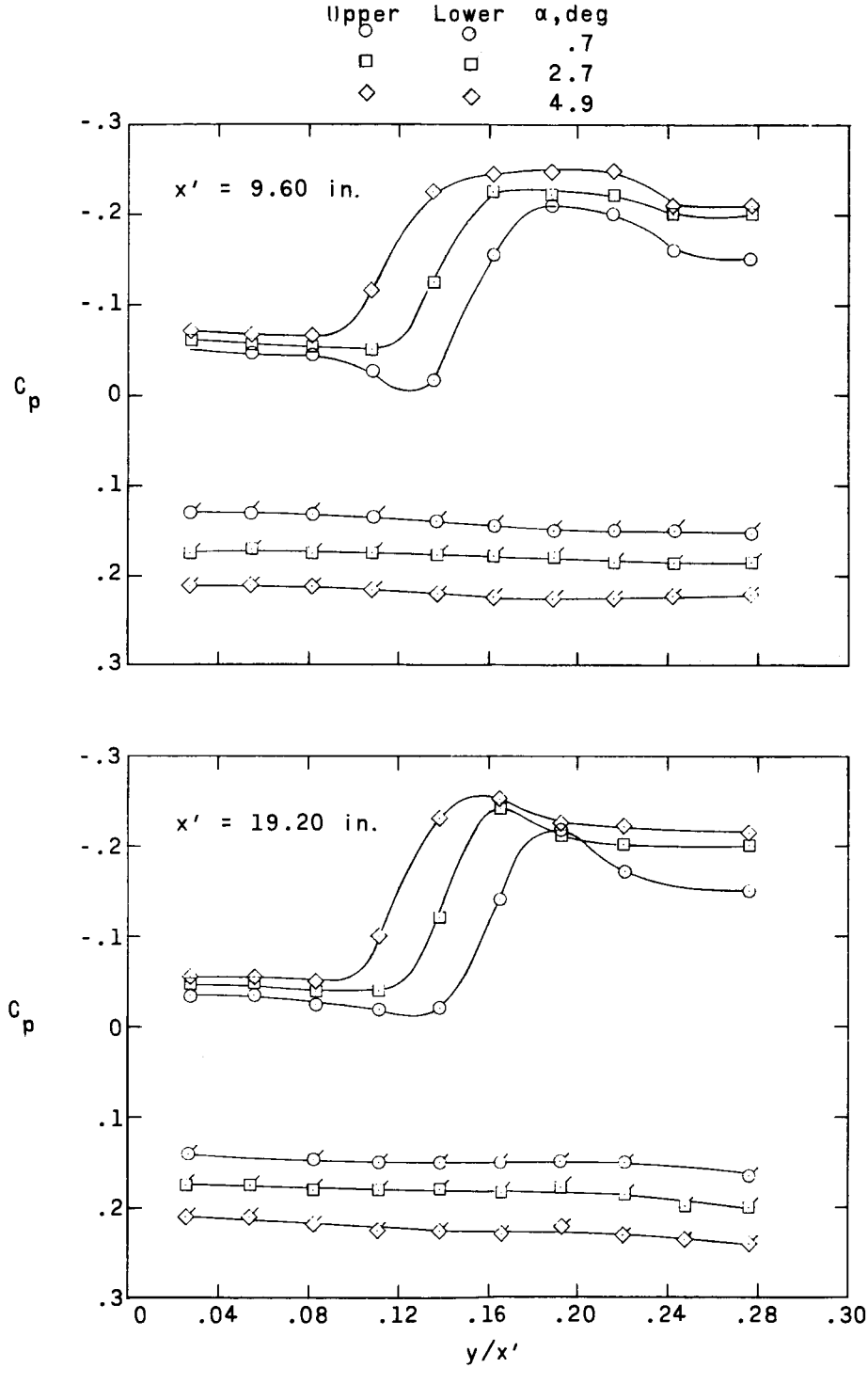

(a) Model A.

Figure 2.- Pressure distributions measured on surface of models.

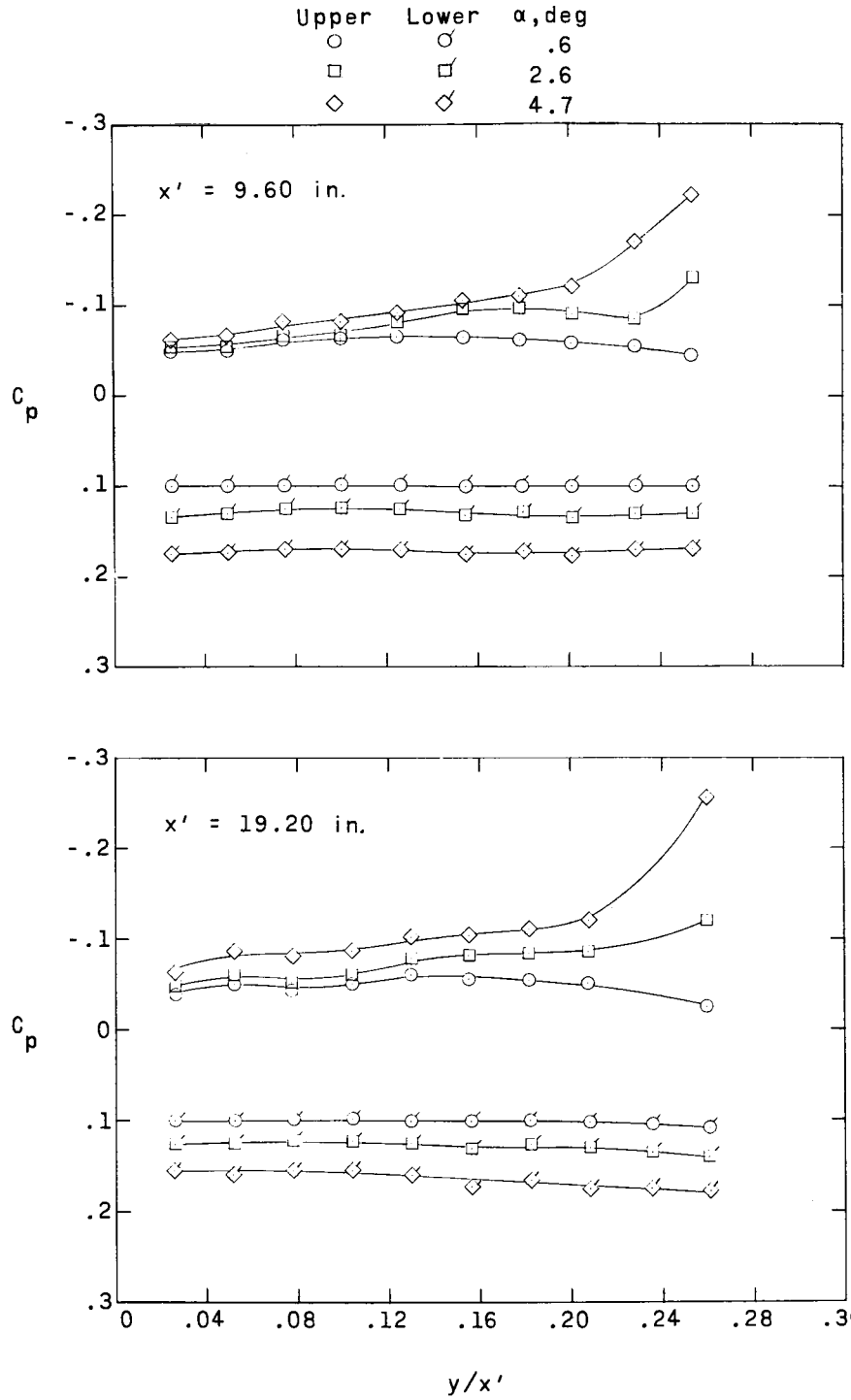

(b) Model B.

Figure 2.- Concluded.

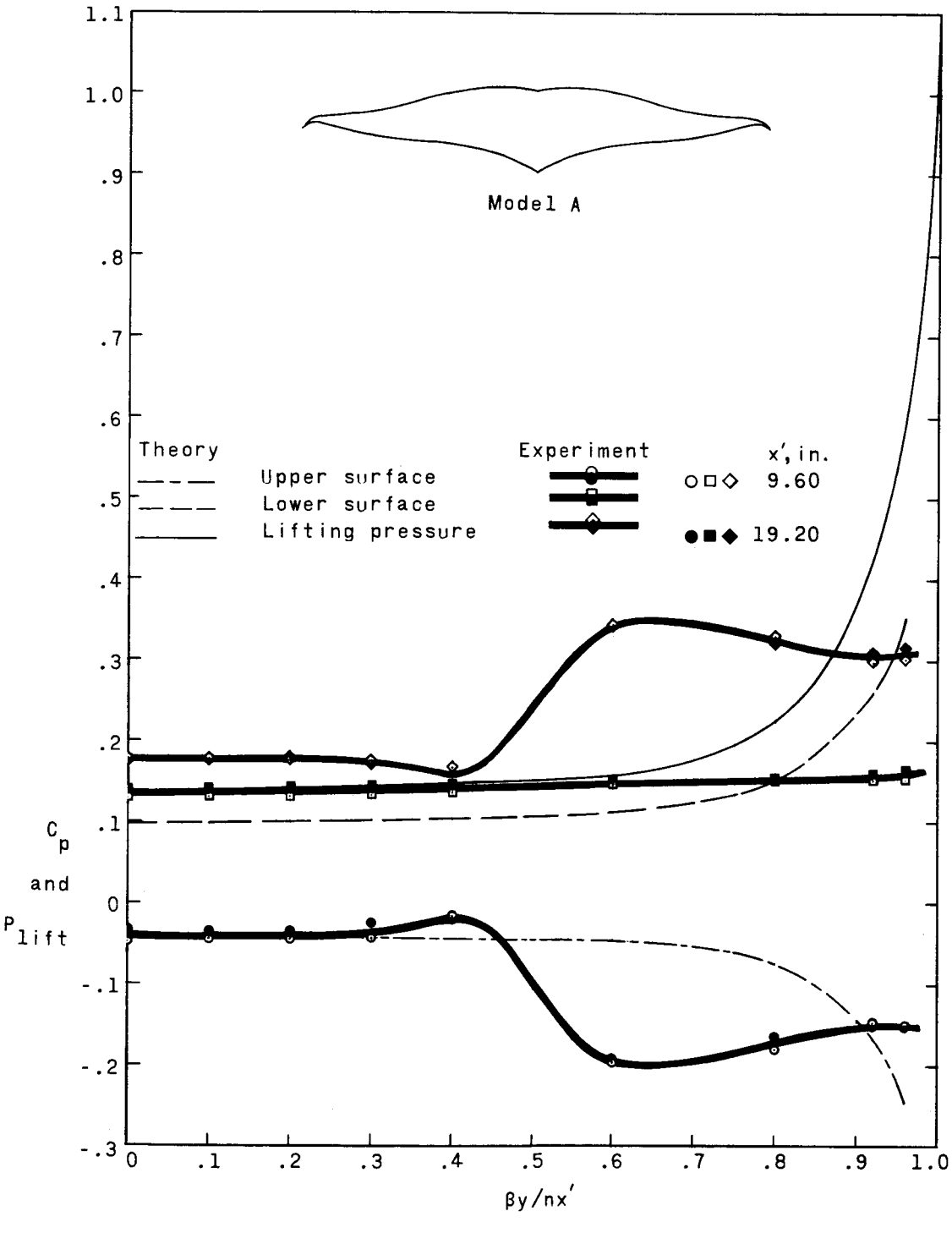

(a) Model A.

Figure 3.- Comparison of the experimental and theoretical surface pressure at $\alpha = 0^{\circ}$.

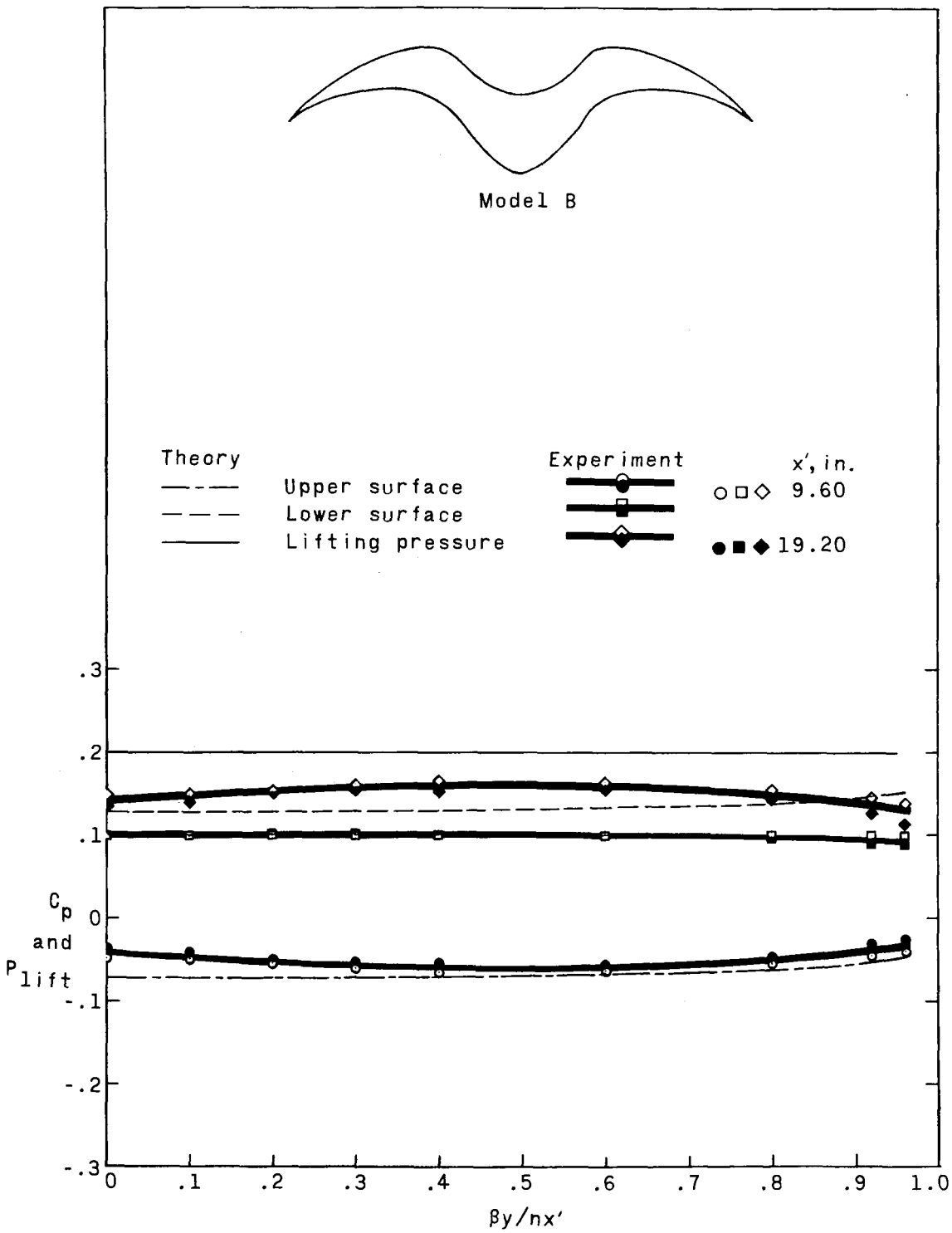

(b) Model B.

Figure 3.- Concluded.

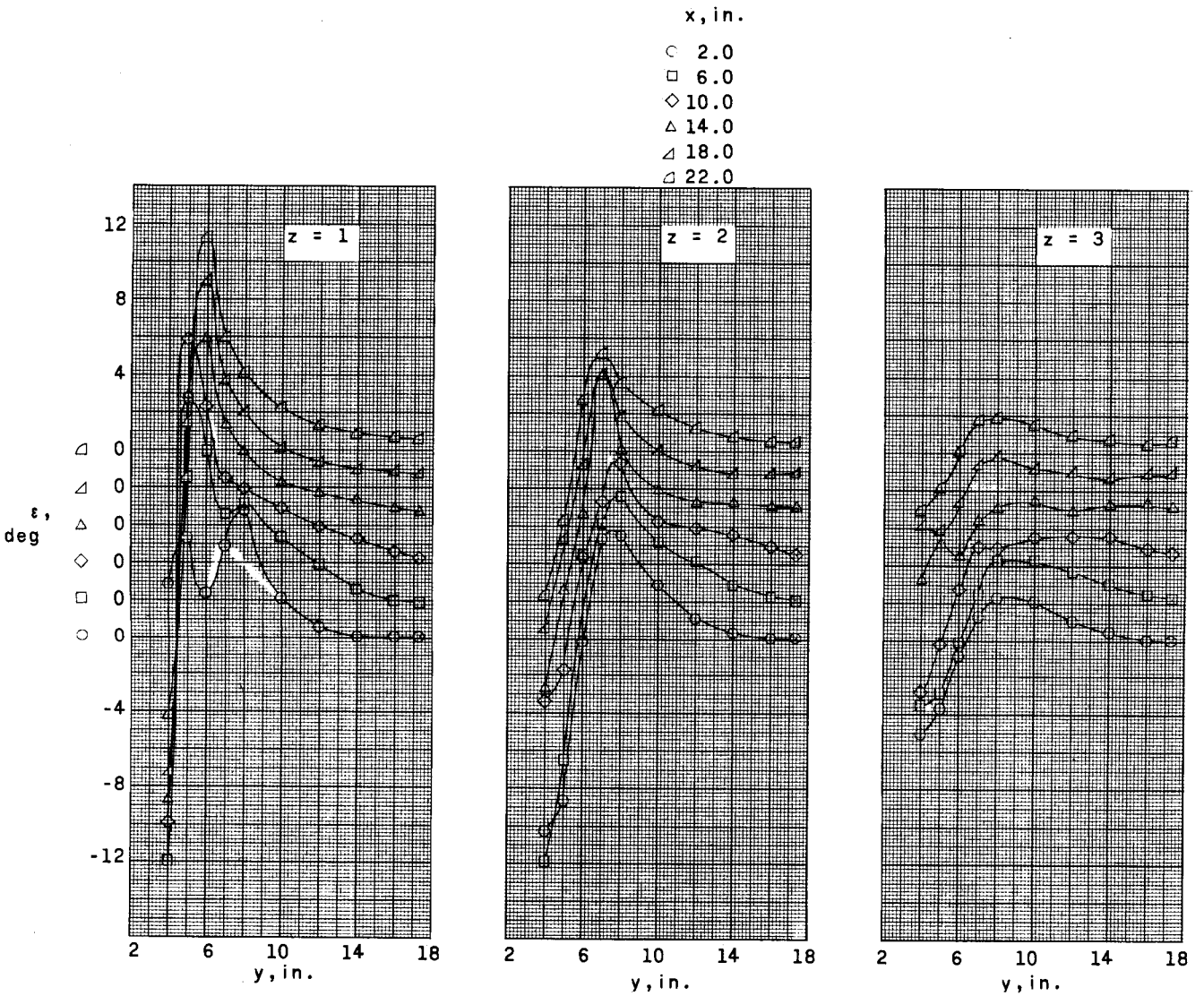

(a) Model A; $\alpha = 0.7^{\circ}$.

Figure 4.- Variation of the local downwash angle with spanwise probe tip position for each chordwise and vertical probe location measured in the model flow field.

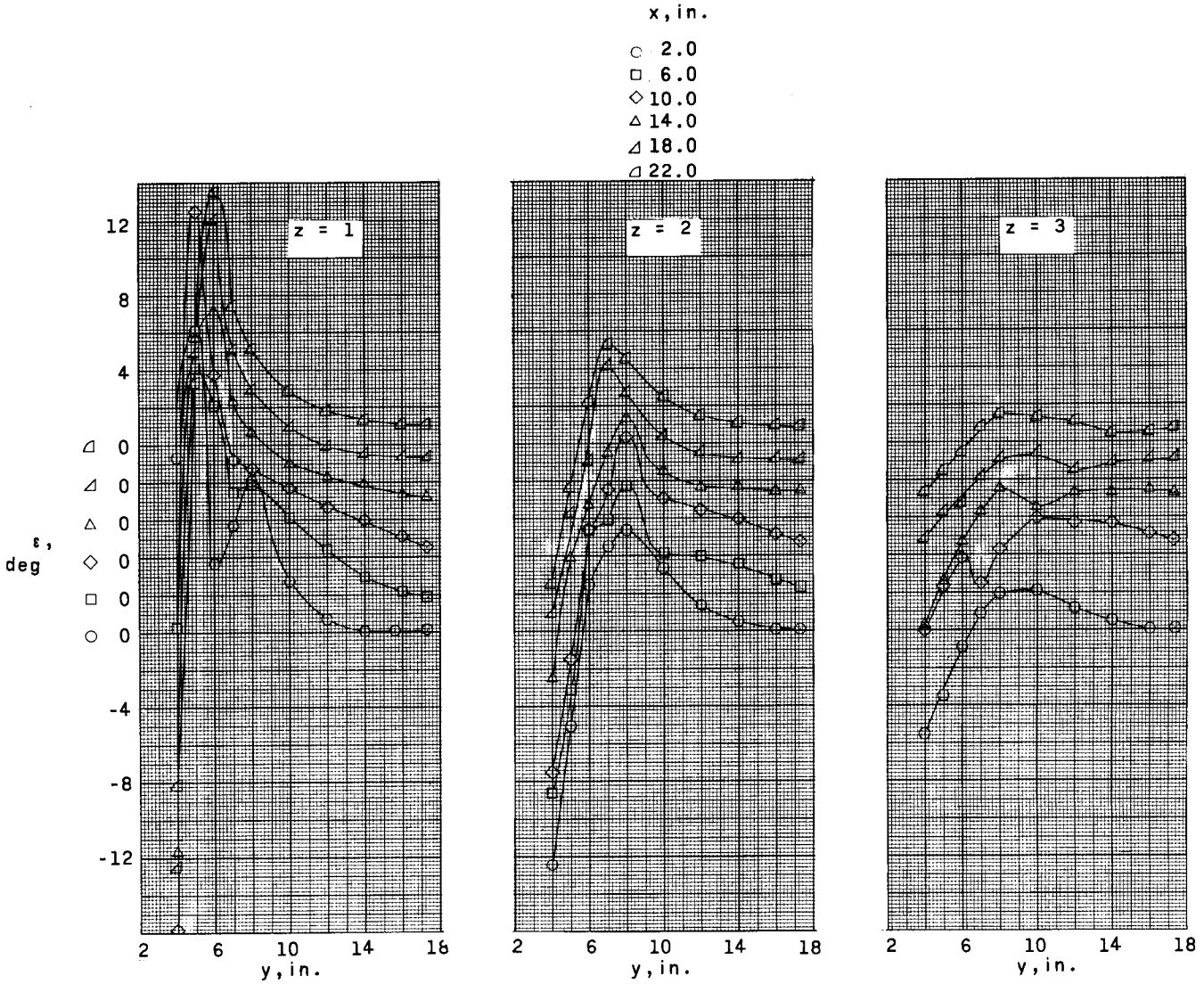

(b) Model A; $\alpha = 2.7^{\circ}$.

Figure 4.- Continued.

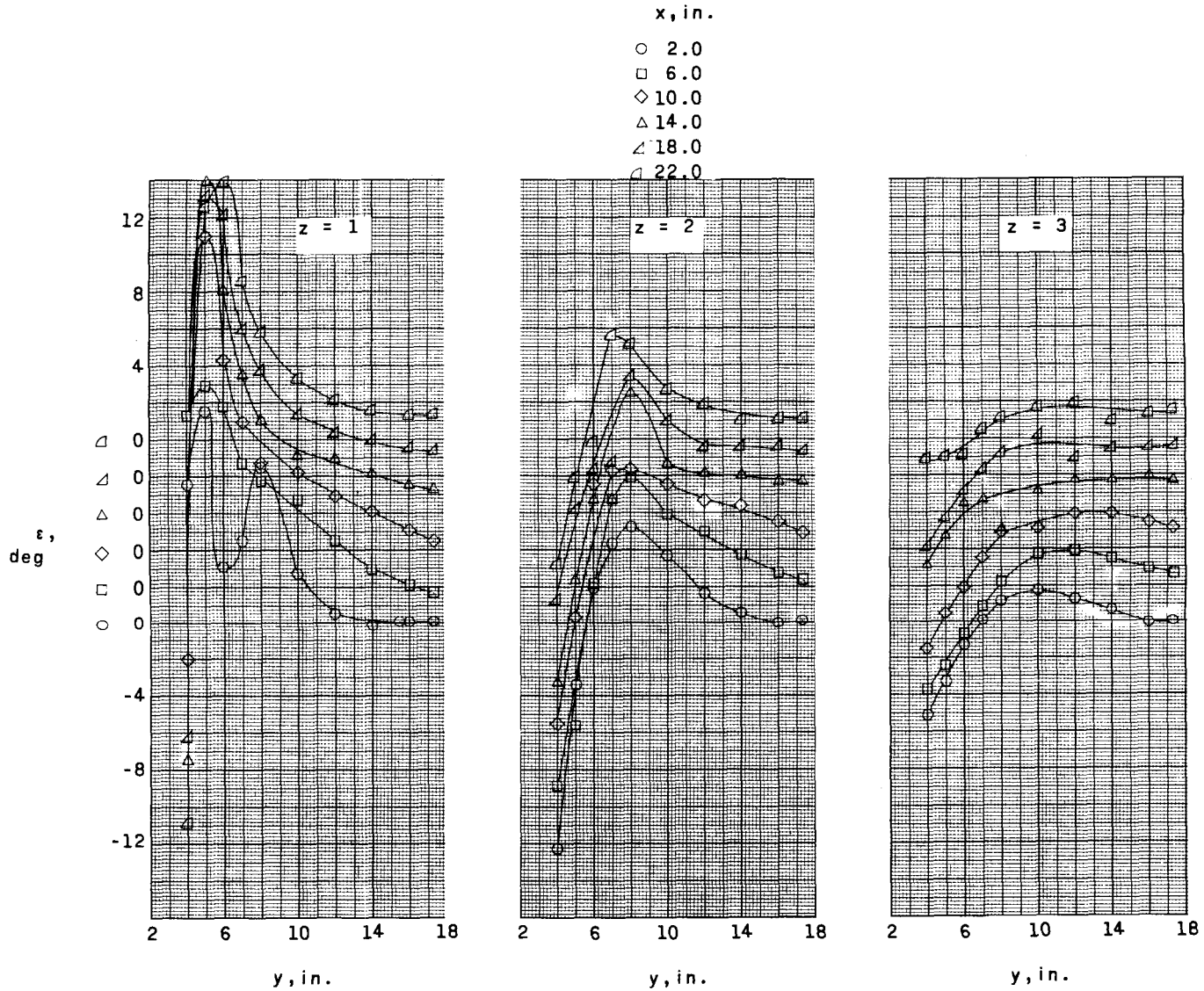

(c) Model A; $\alpha = 4.9^{\circ}$.

Figure 4.- Continued.

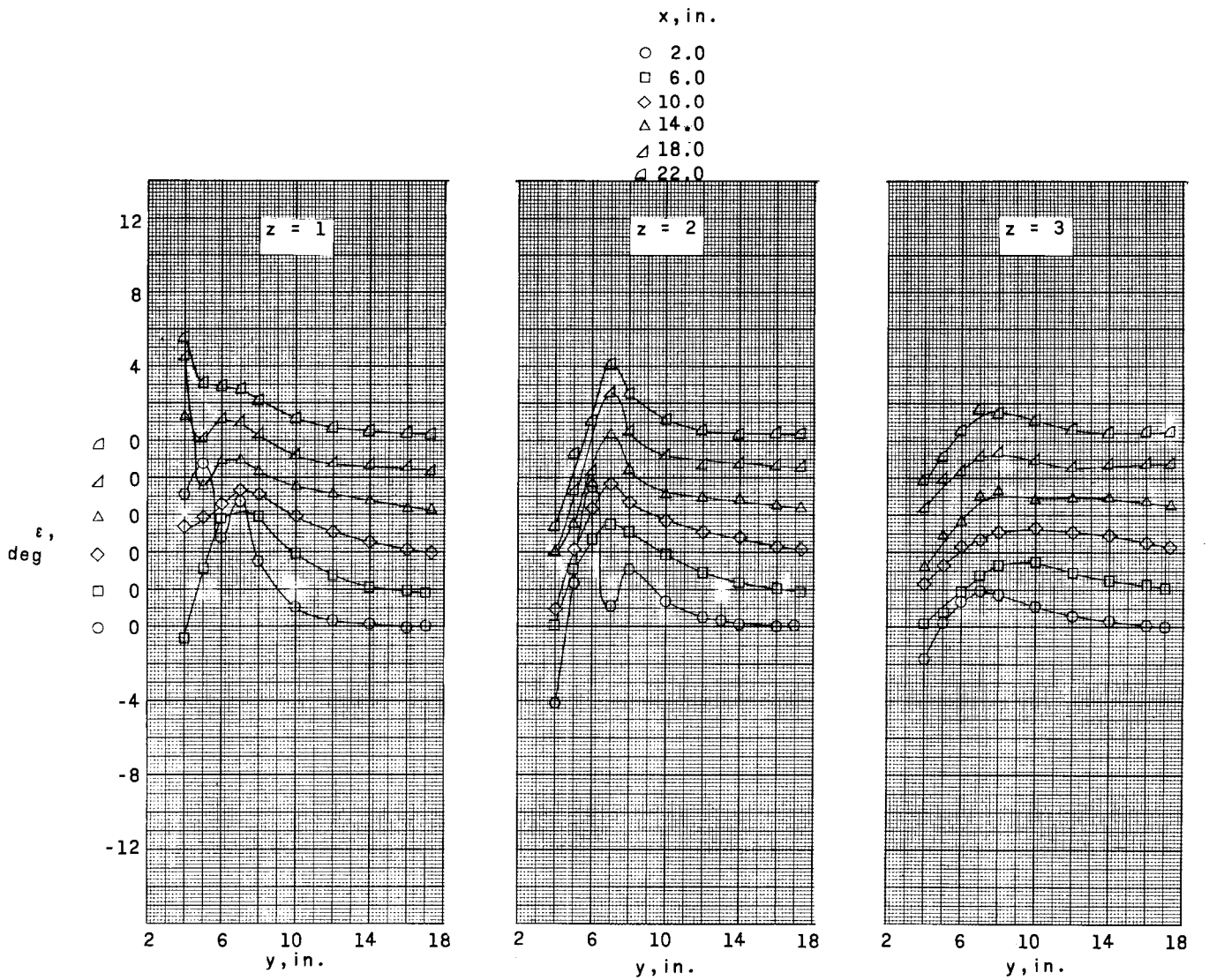

(d) Model B; $\alpha = 0.6°$.

Figure 4.- Continued.

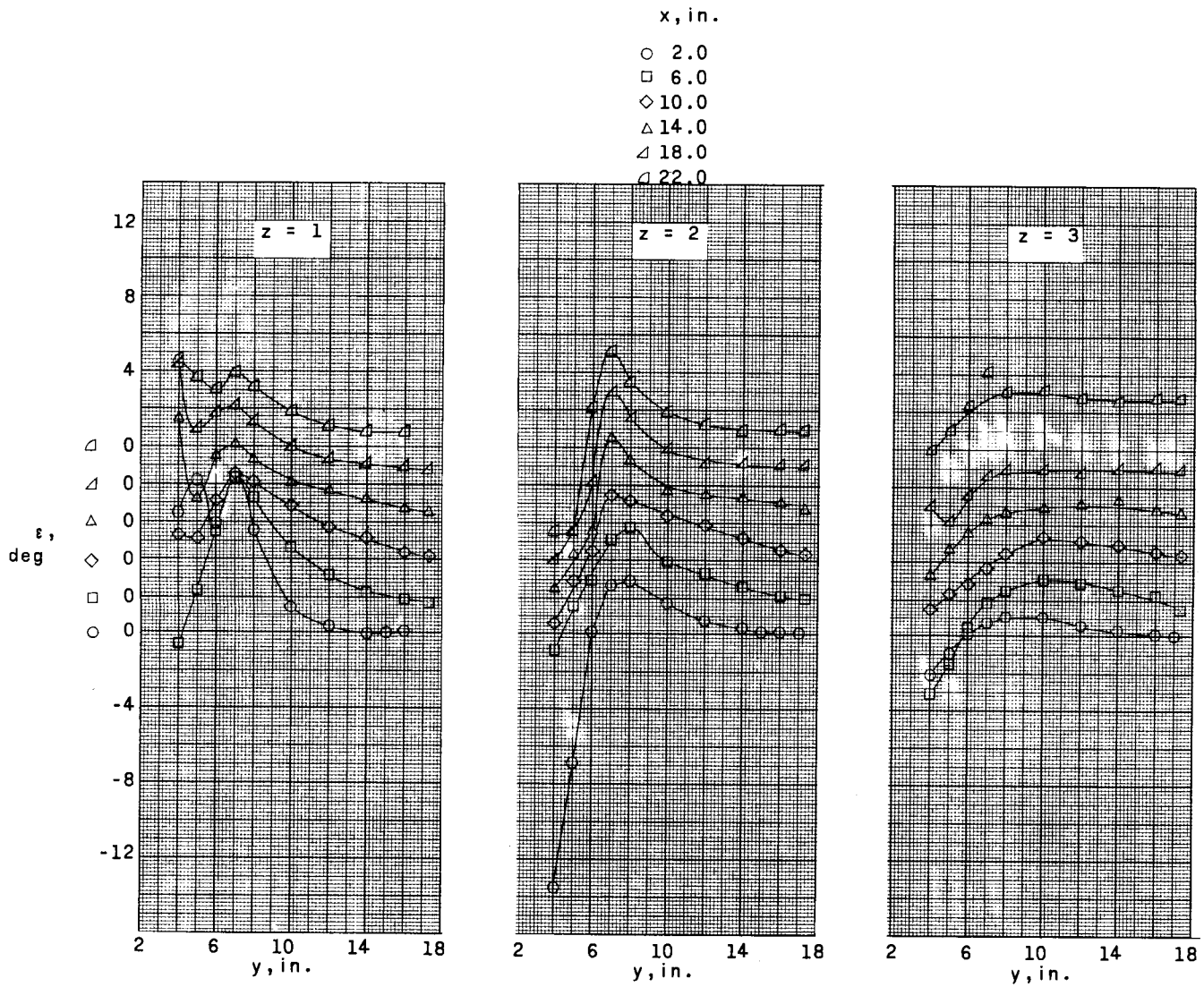

(e) Model B; $\alpha = 2.6^{\circ}$.

Figure 4.- Continued.

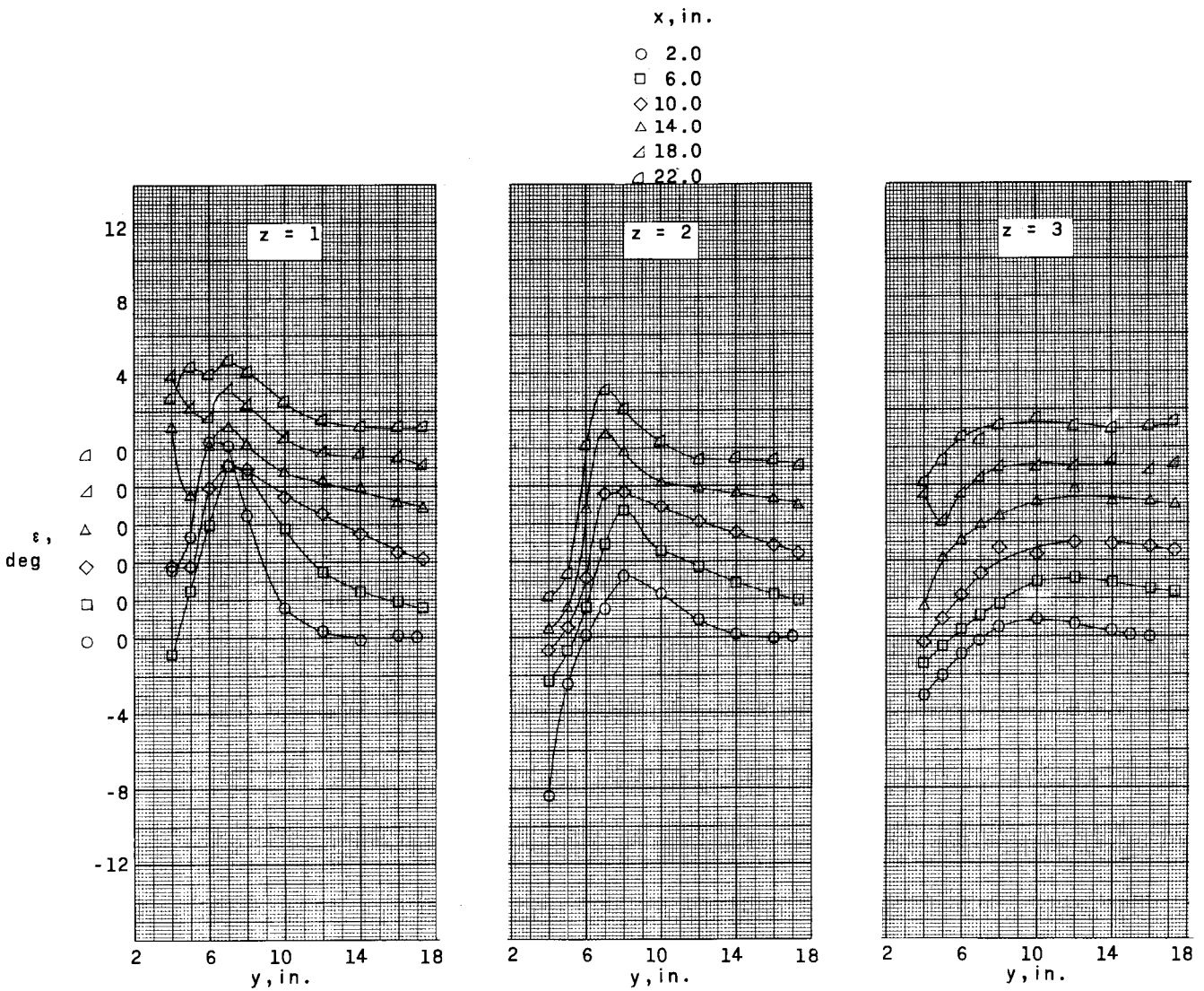

(f) Model B; $\alpha = 4.7^{\circ}$.

Figure 4.- Concluded.

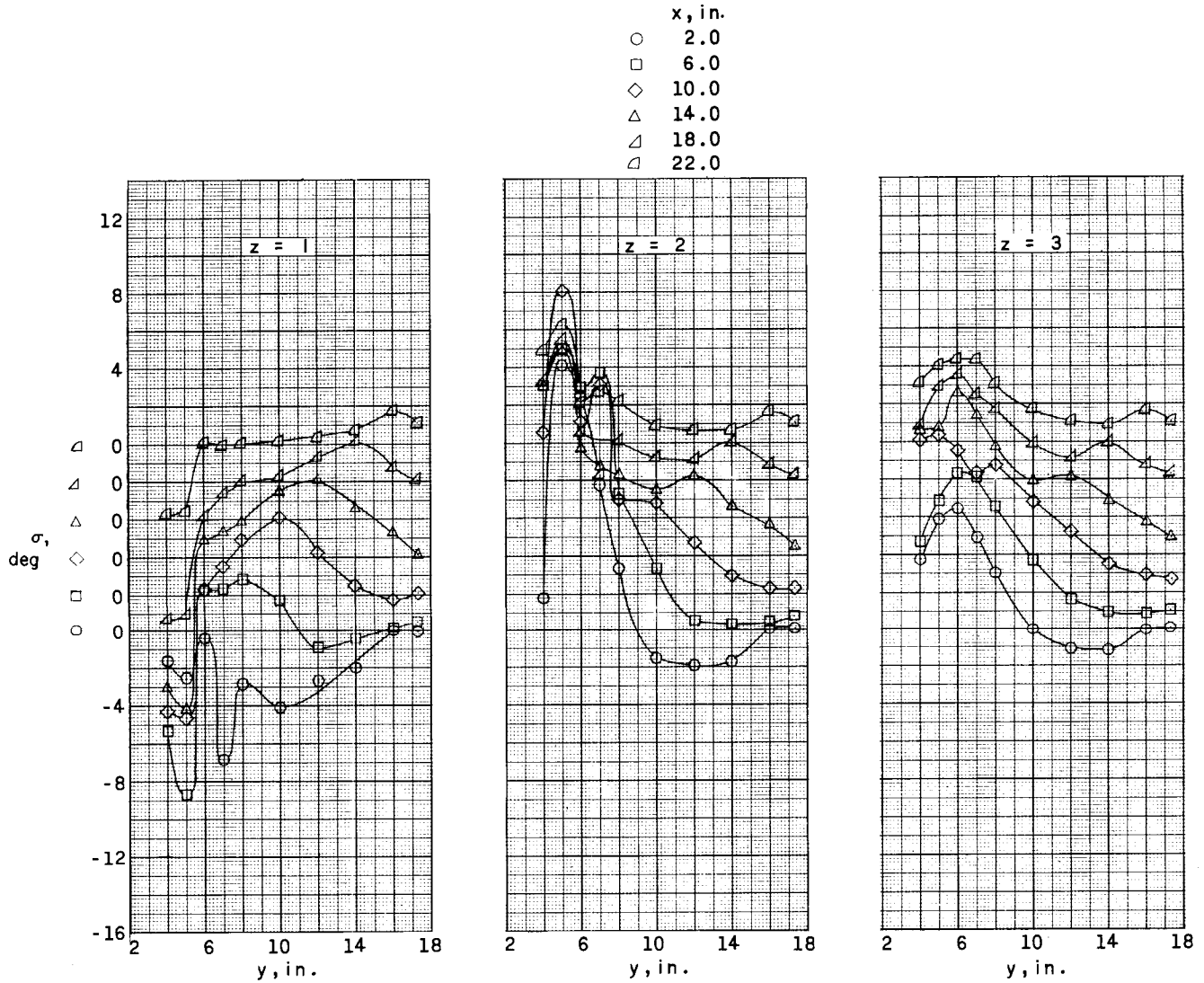

(a) Model A; $\alpha = 0.7^{\circ}$.

Figure 5.- Variation of the local sidewash angle with spanwise probe tip position for each chordwise and vertical probe location measured in the model flow field.

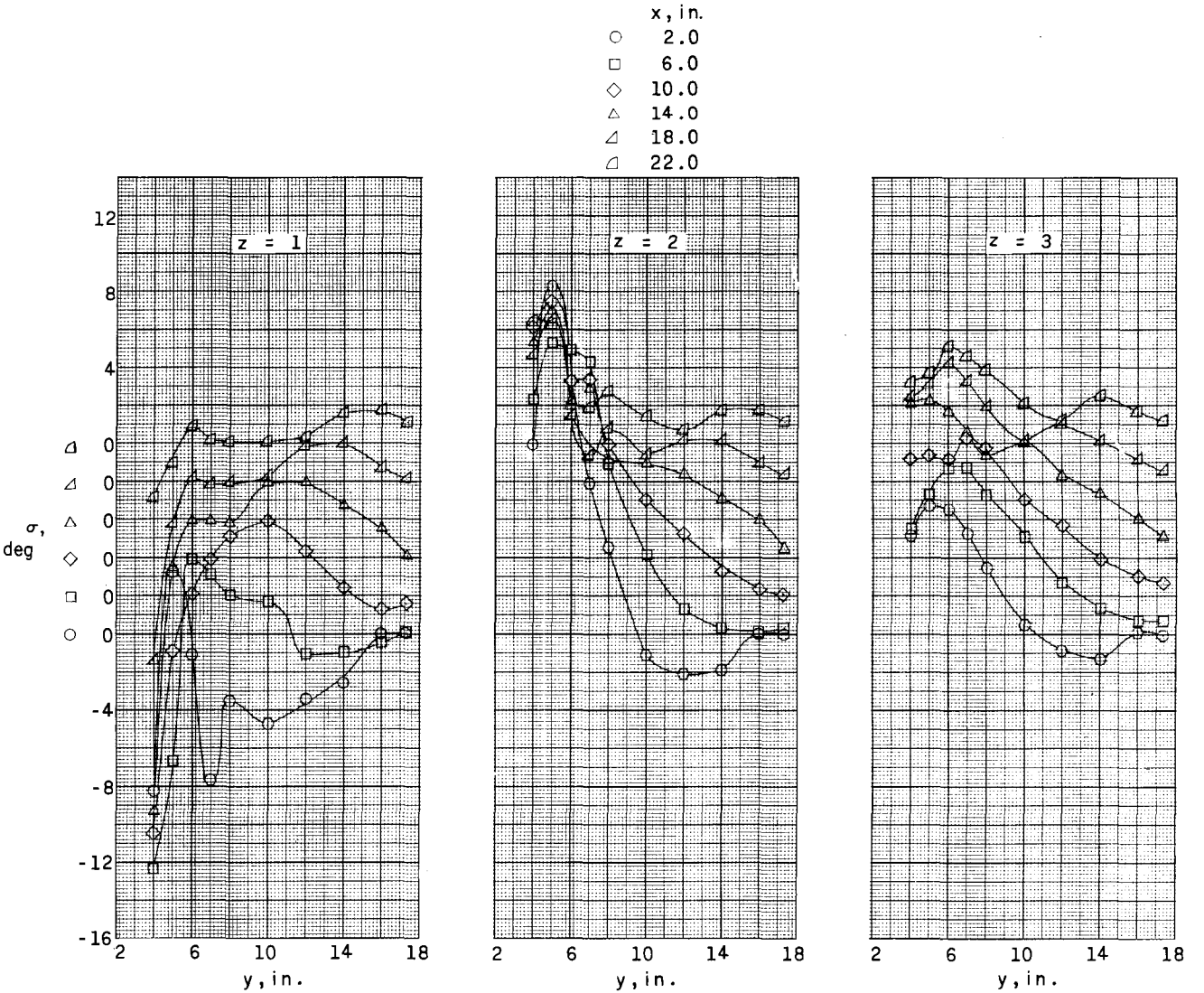

(b) Model A; $\alpha = 2.7^{\circ}$.

Figure 5.- Continued.

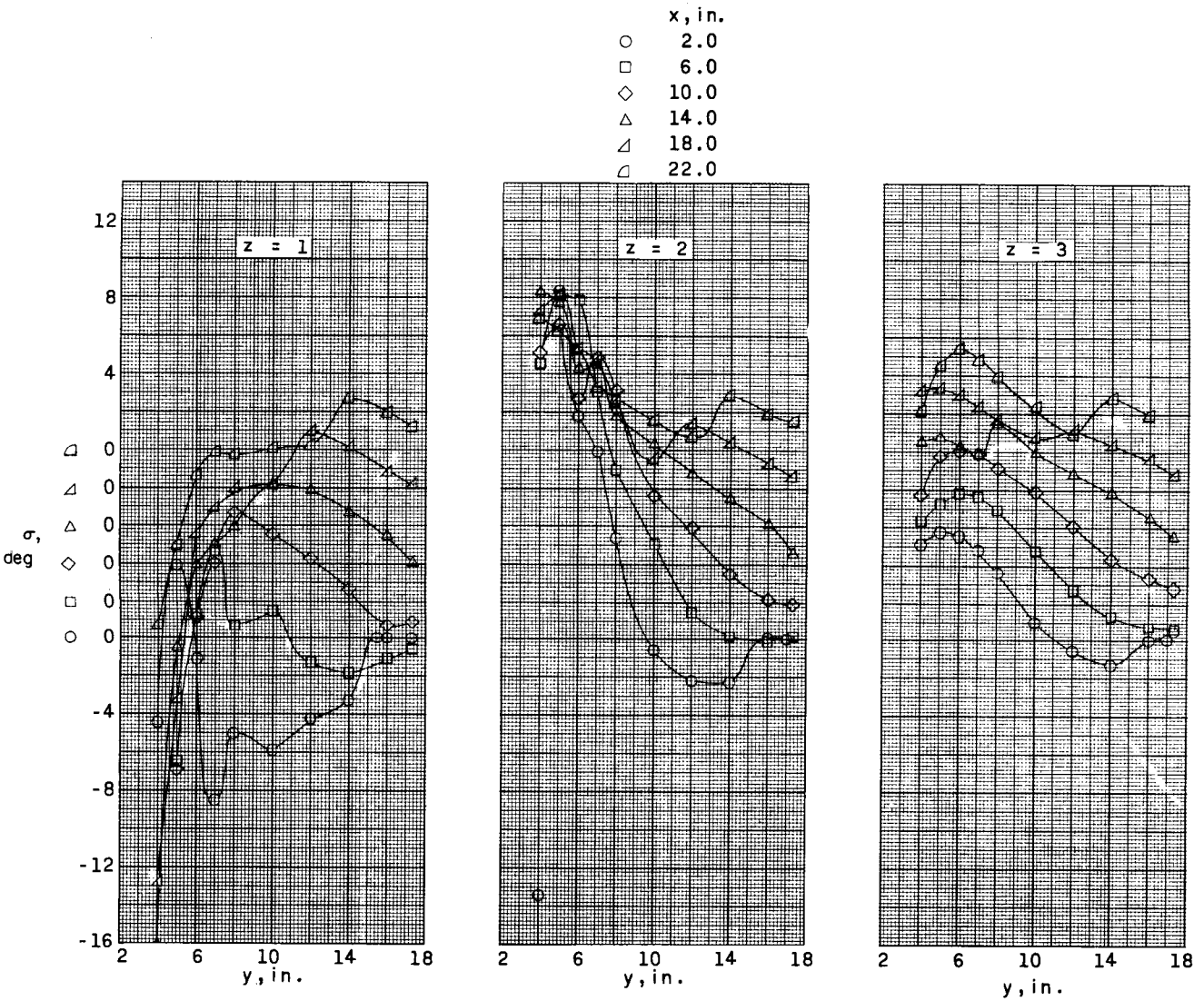

(c) Model A; $\alpha = 4.9^{\circ}$.

Figure 5.- Continued.

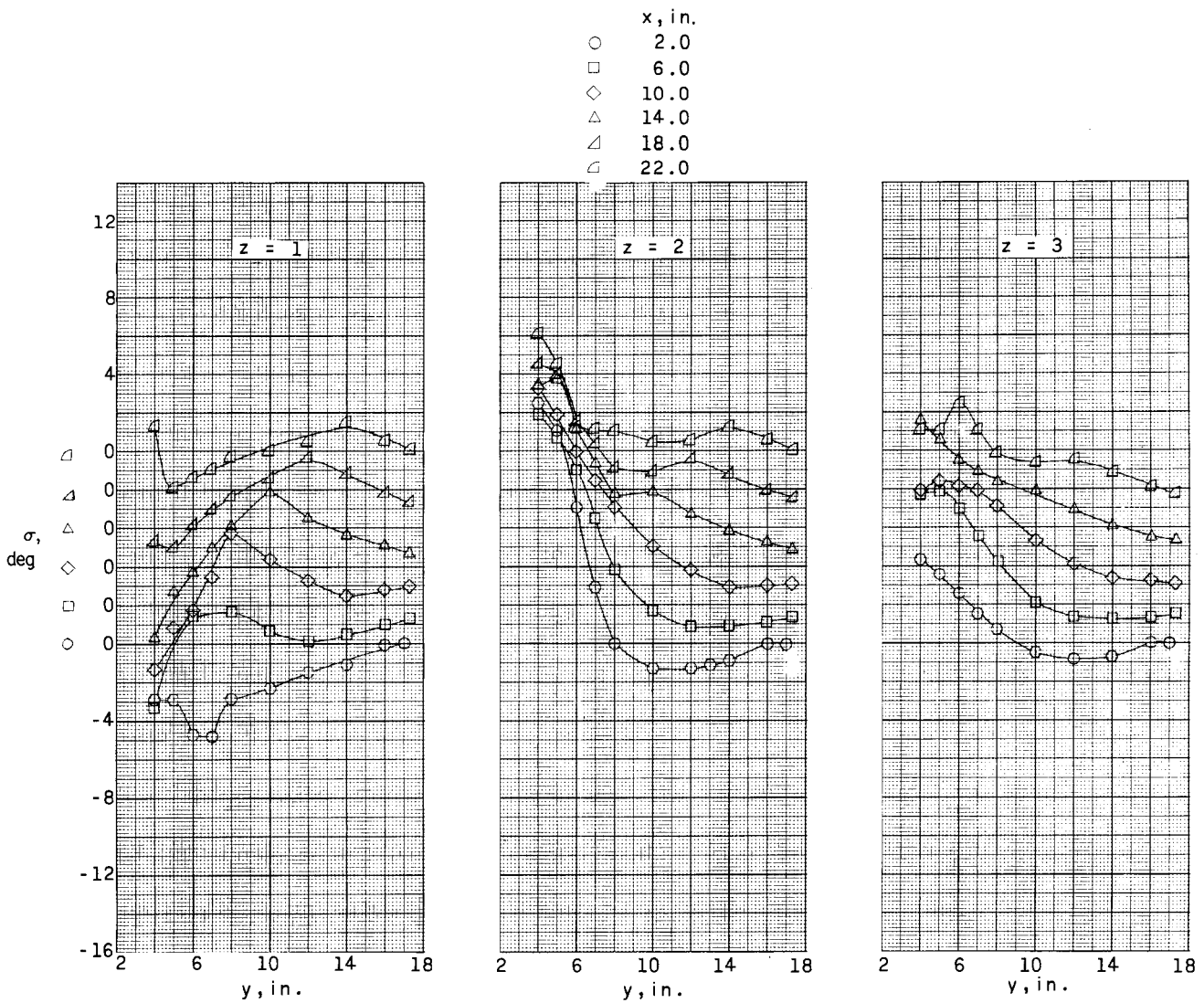

(d) Model B; $\alpha = 0.6^{\circ}$.

Figure 5.- Continued.

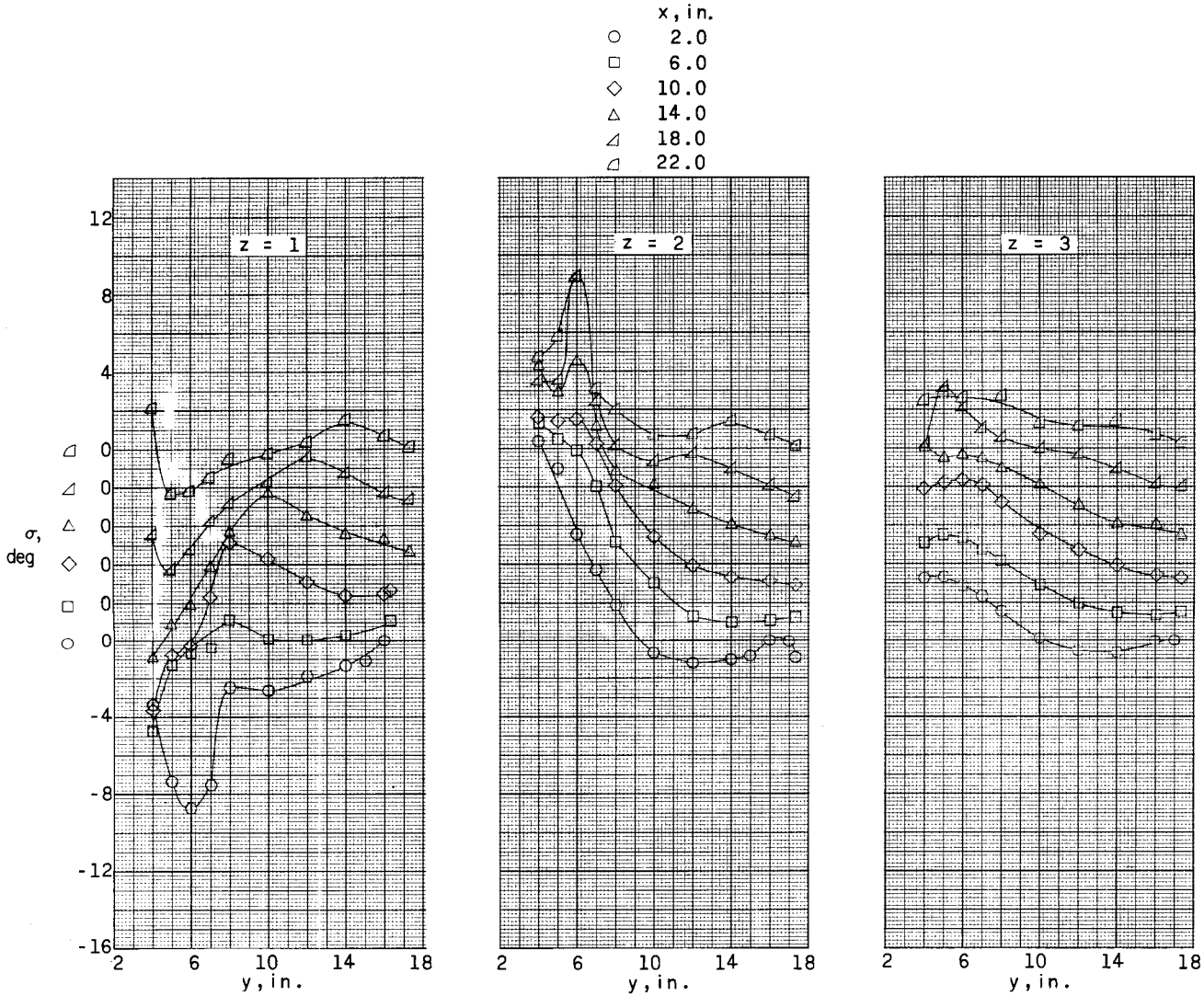

(e) Model B; $\alpha = 2.6^{\circ}$.

Figure 5.- Continued.

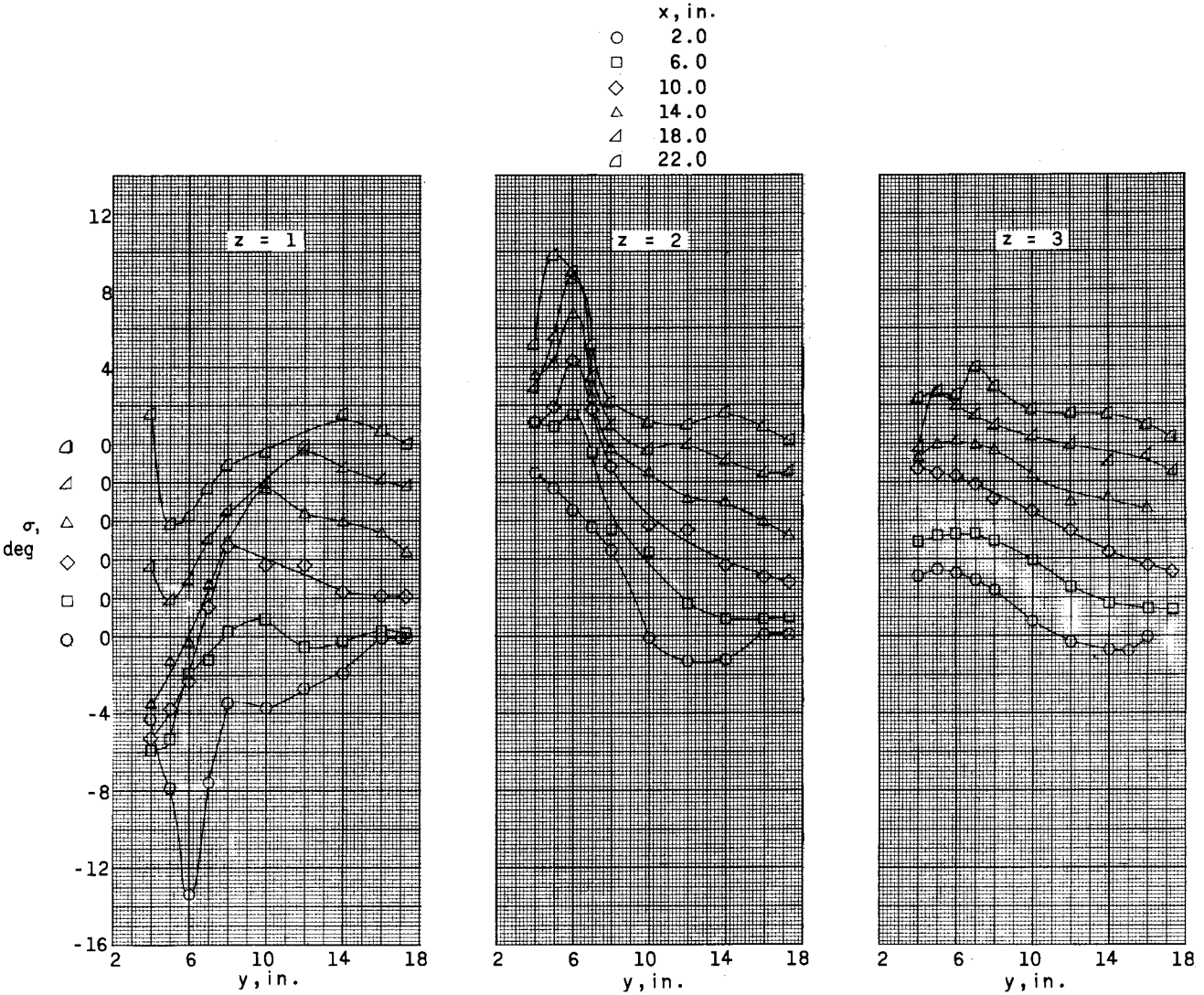

(f) Model B; $\alpha = 4.7^{\circ}$.

Figure 5.- Concluded.

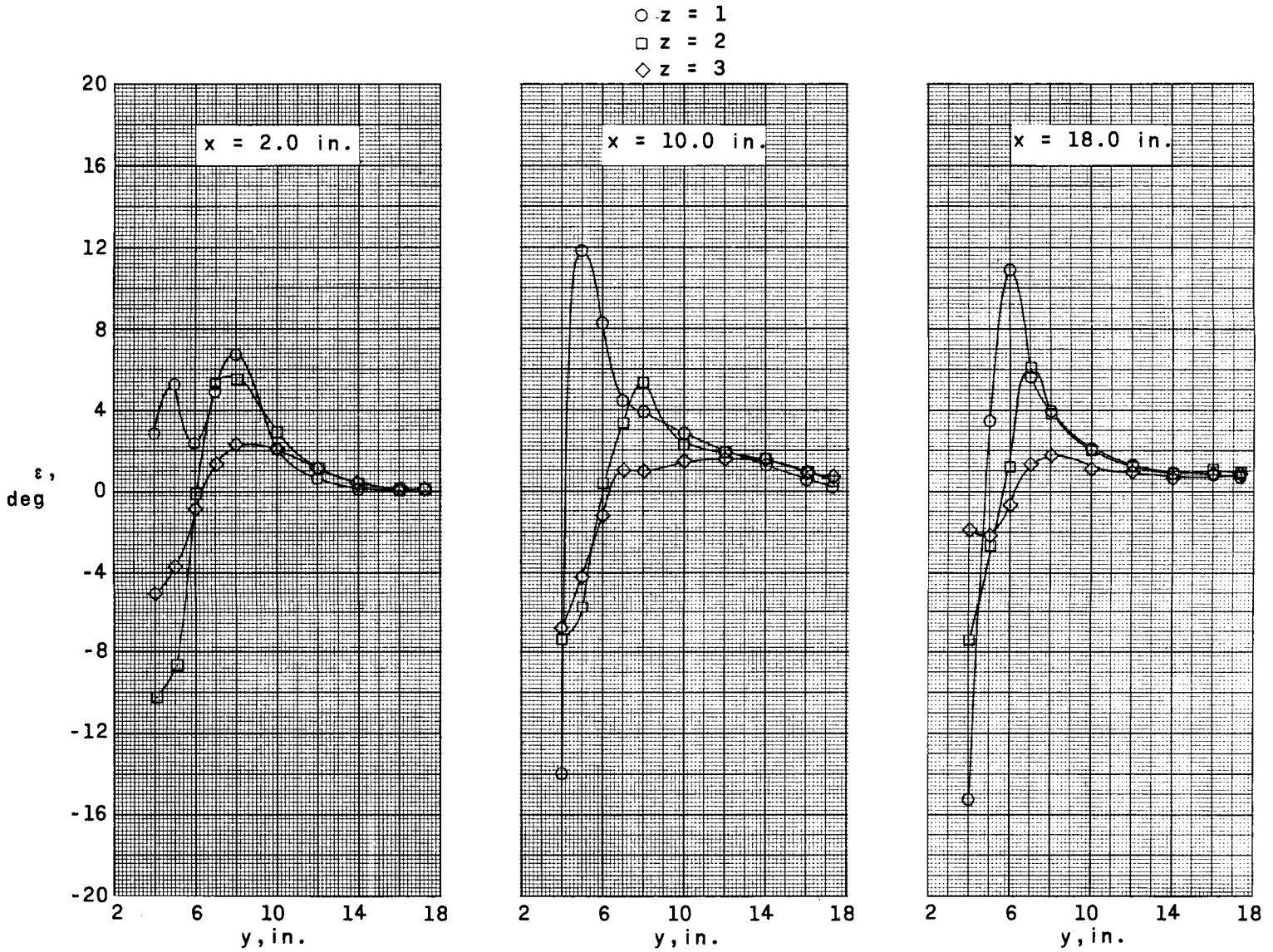

(a) Model A; $\alpha = 0.7^{\circ}$.

Figure 6.- Effect of probe vertical position on the local downwash angle for various spanwise and chordwise probe positions.

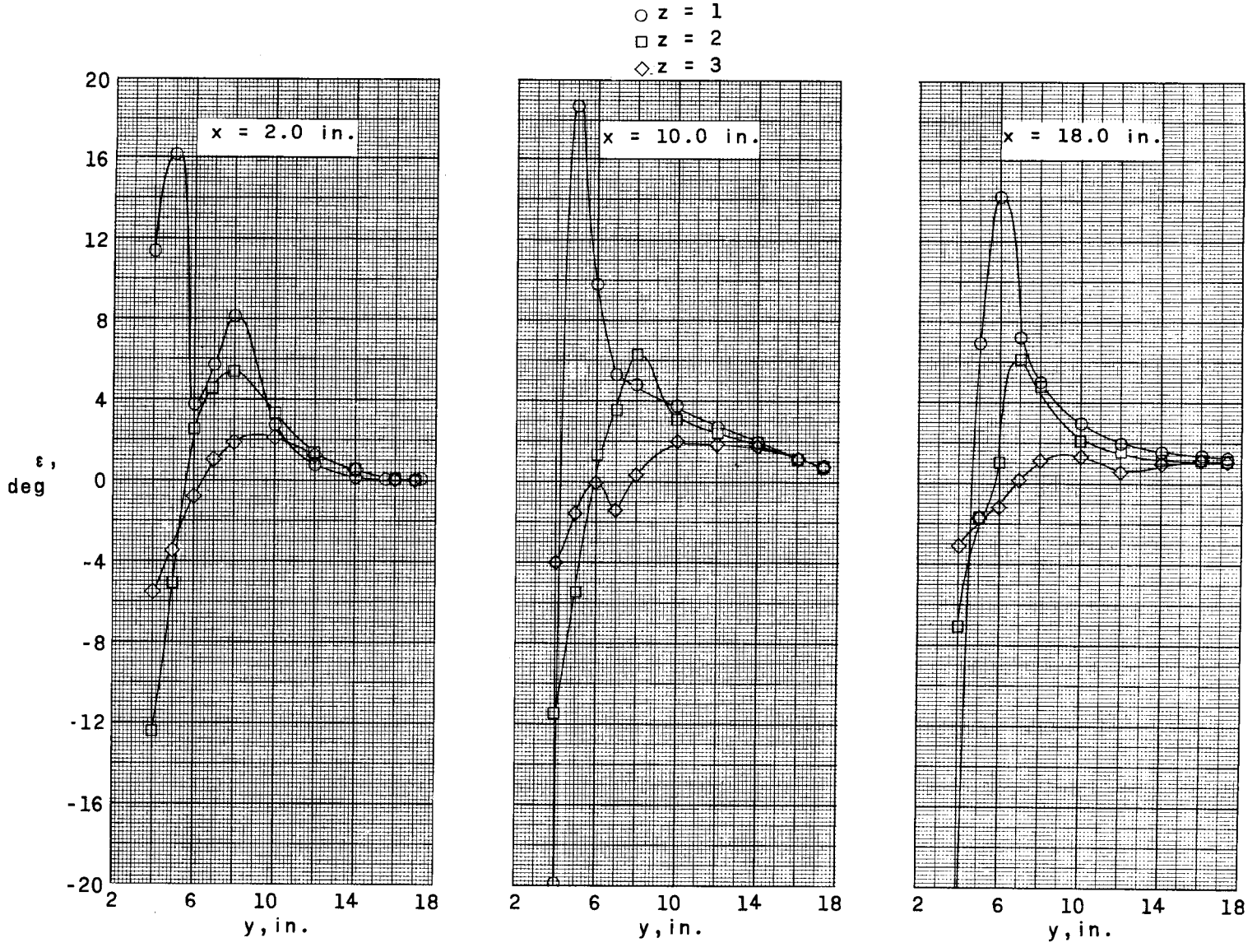

(b) Model A; $\alpha = 2.7^{\circ}$.

Figure 6.- Continued.

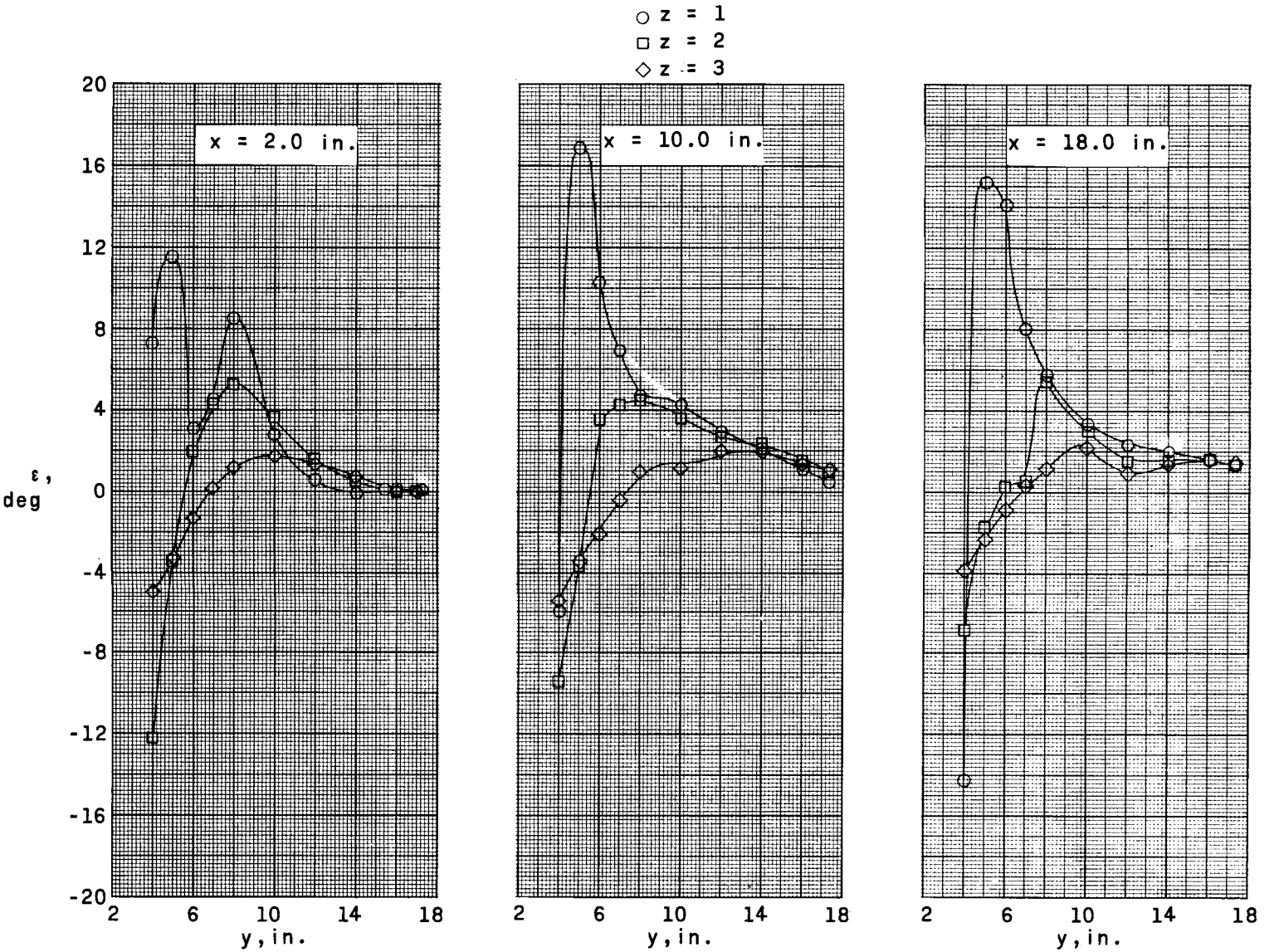

(c) Model A; $\alpha = 4.9^{\circ}$.

Figure 6.- Continued.

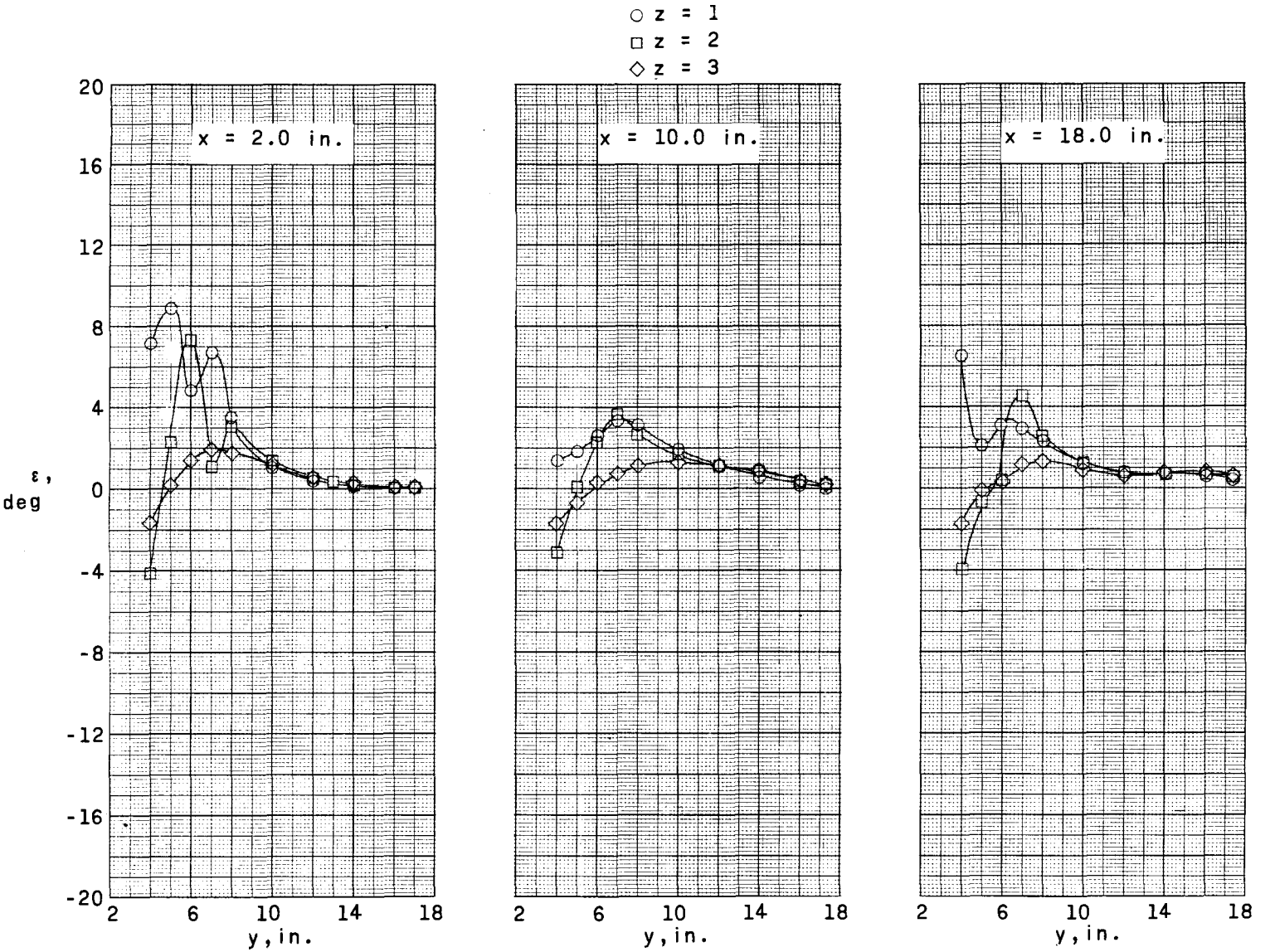

(d) Model B; $\alpha = 0.6^{\circ}$.

Figure 6.- Continued.

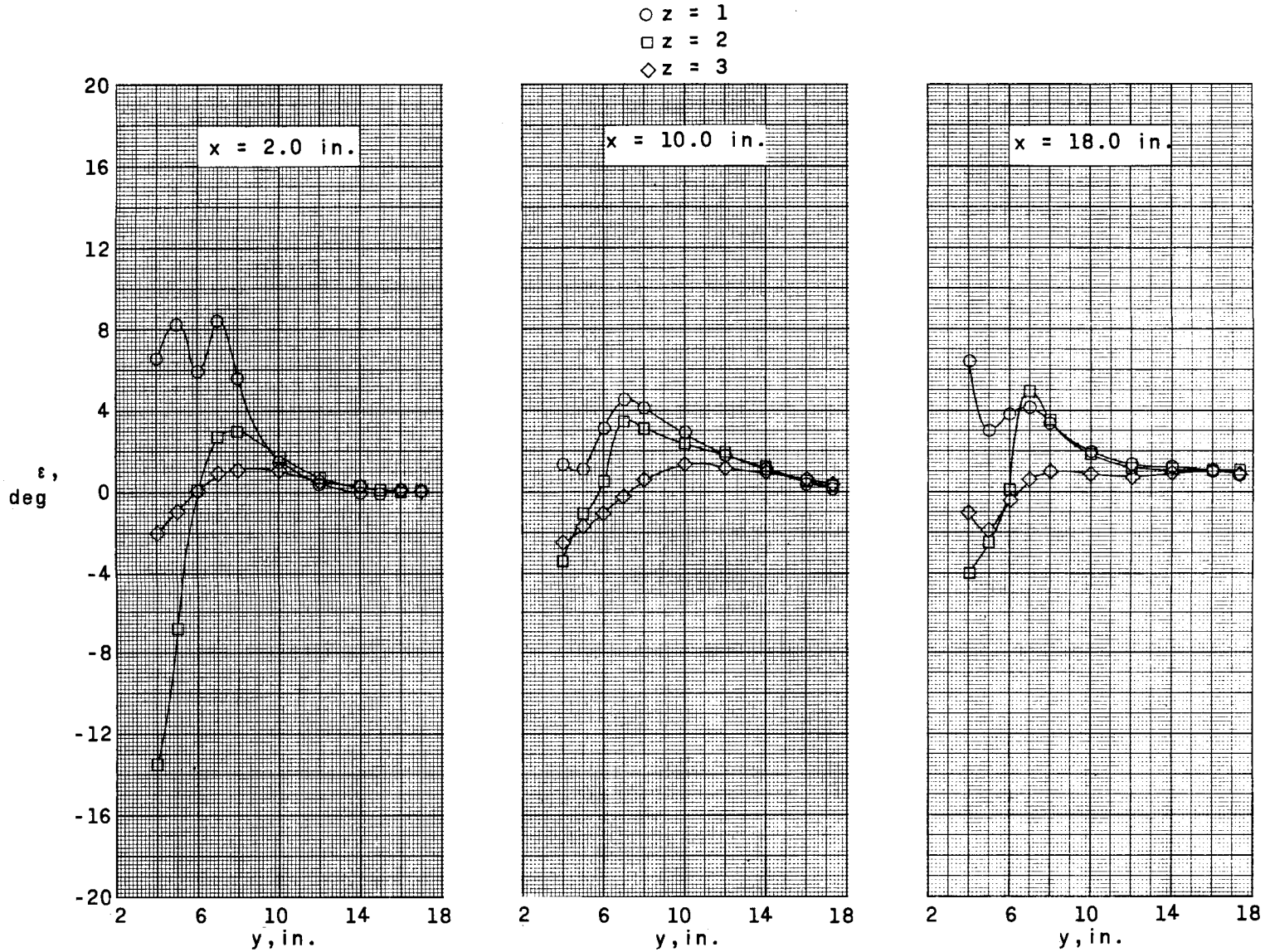

(e) Model B; $\alpha = 2.6^{\circ}$.

Figure 6.- Continued.

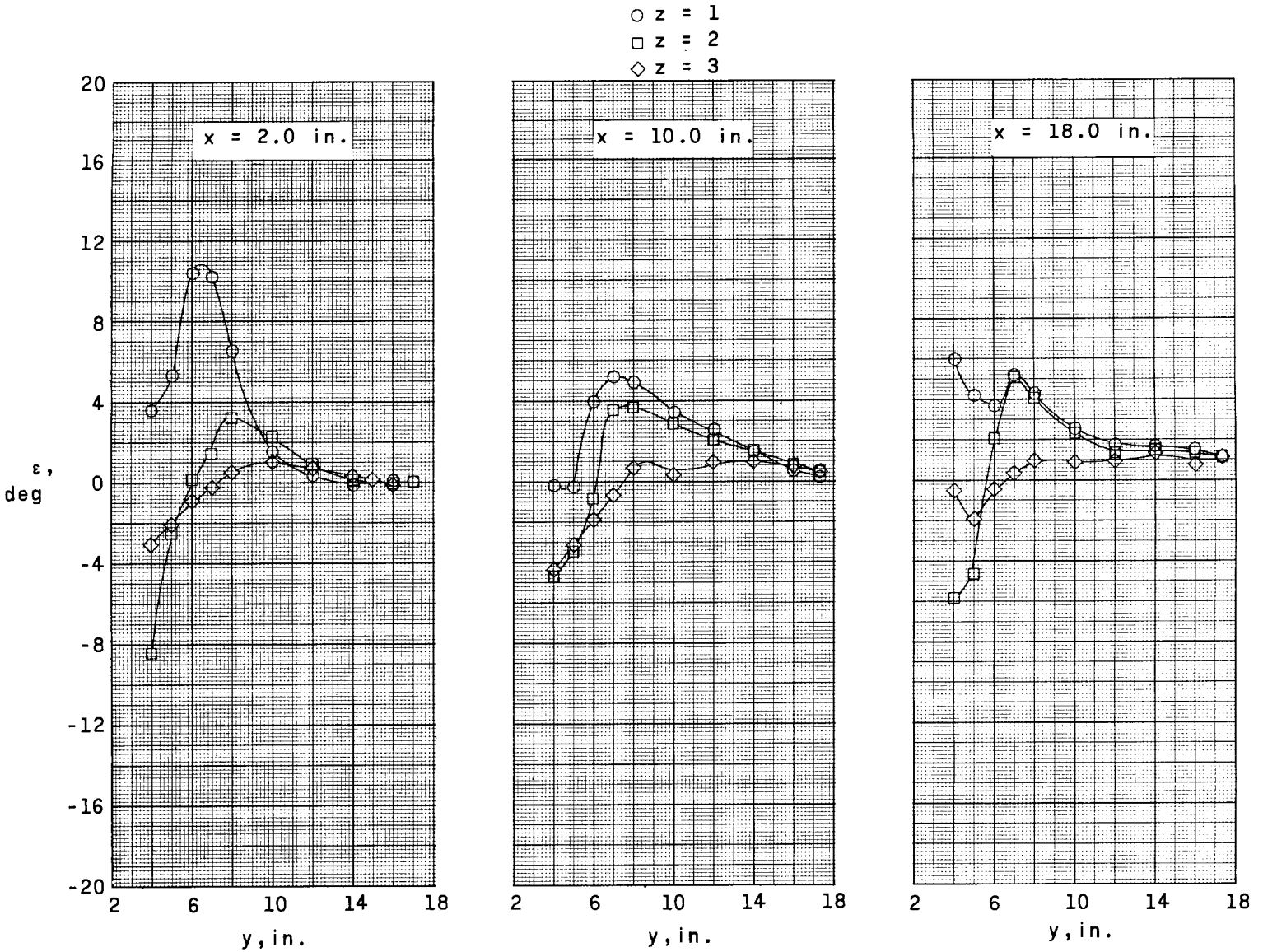

(f) Model B; $\alpha = 4.7^{o}$.

Figure 6.- Concluded.

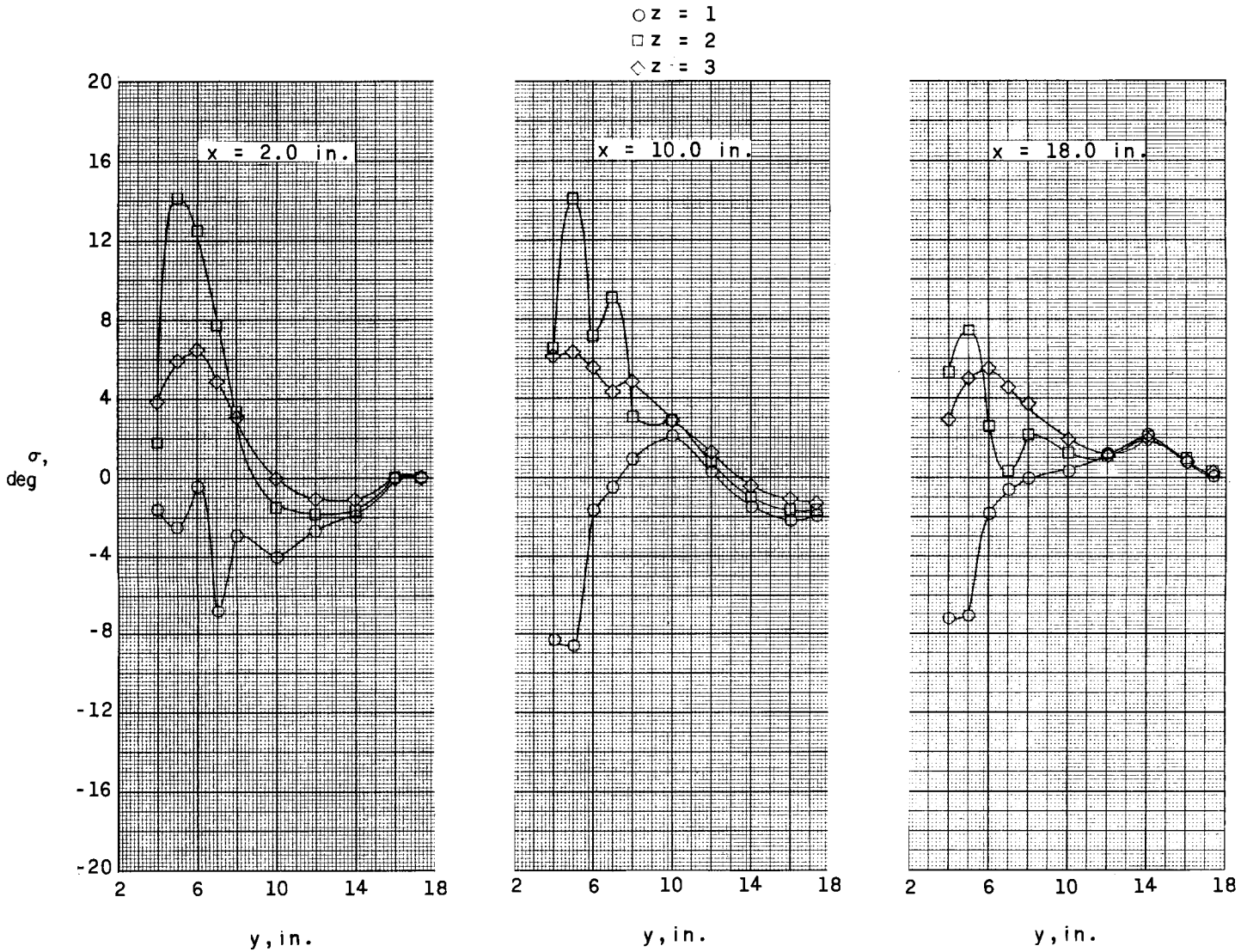

(a) Model A; $\alpha = 0.7^{\circ}$.

Figure 7.- Effect of probe vertical position on the local sidewash angle for various spanwise and chordwise probe positions.

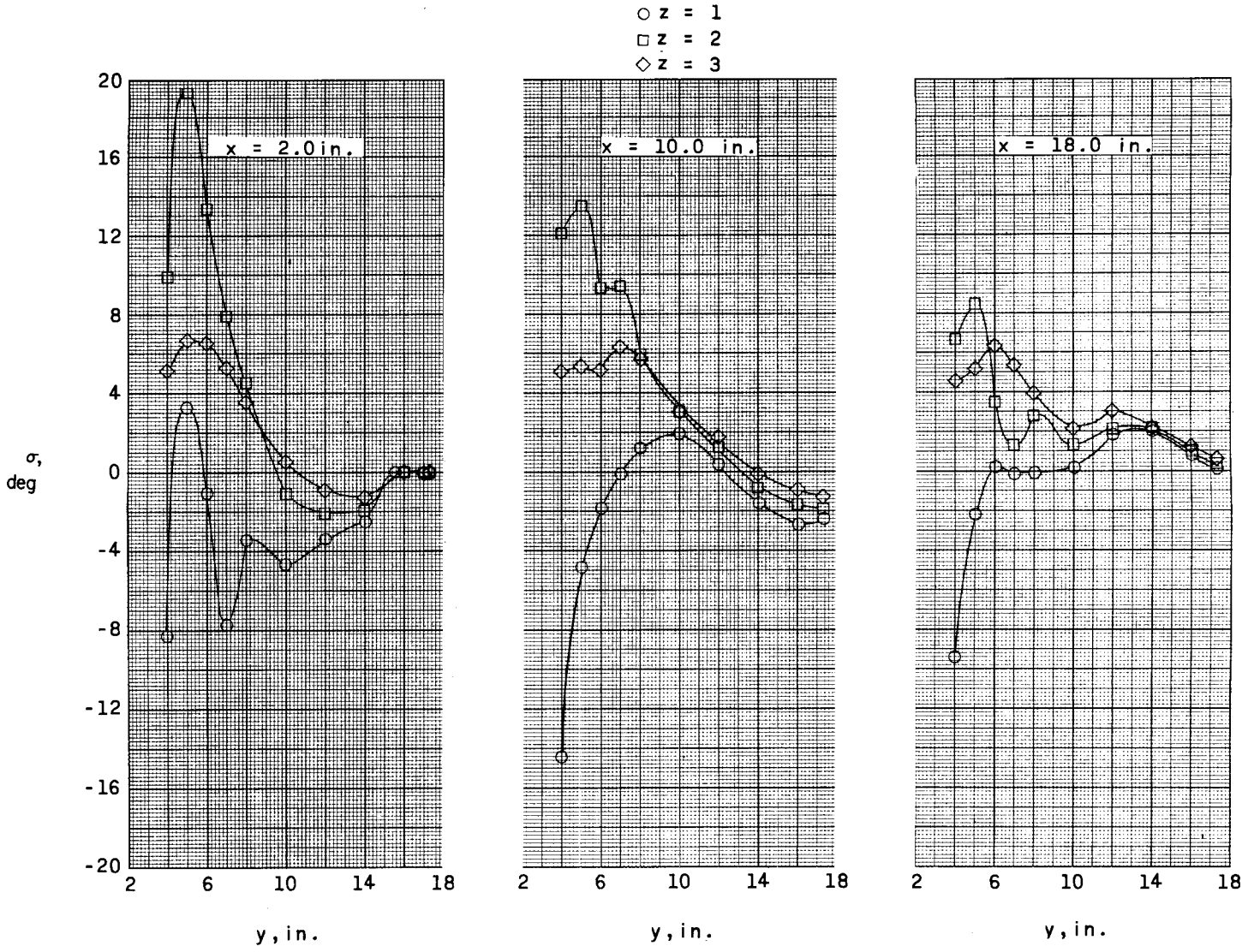

(b) Model A; $\alpha = 2.7^{\circ}$.

Figure 7.- Continued.

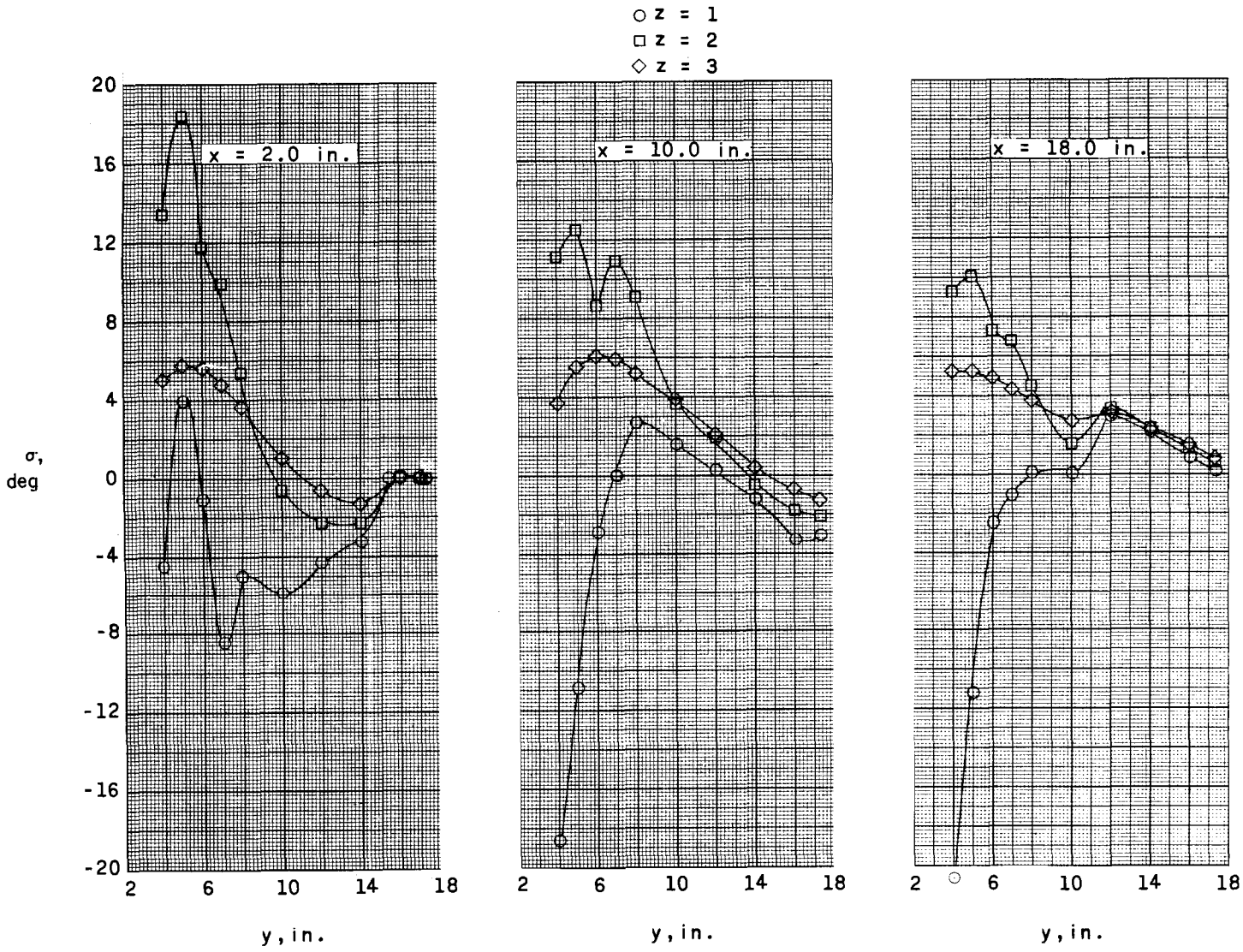

(c) Model A; $\alpha = 4.9^{\circ}$.

Figure 7.- Continued.

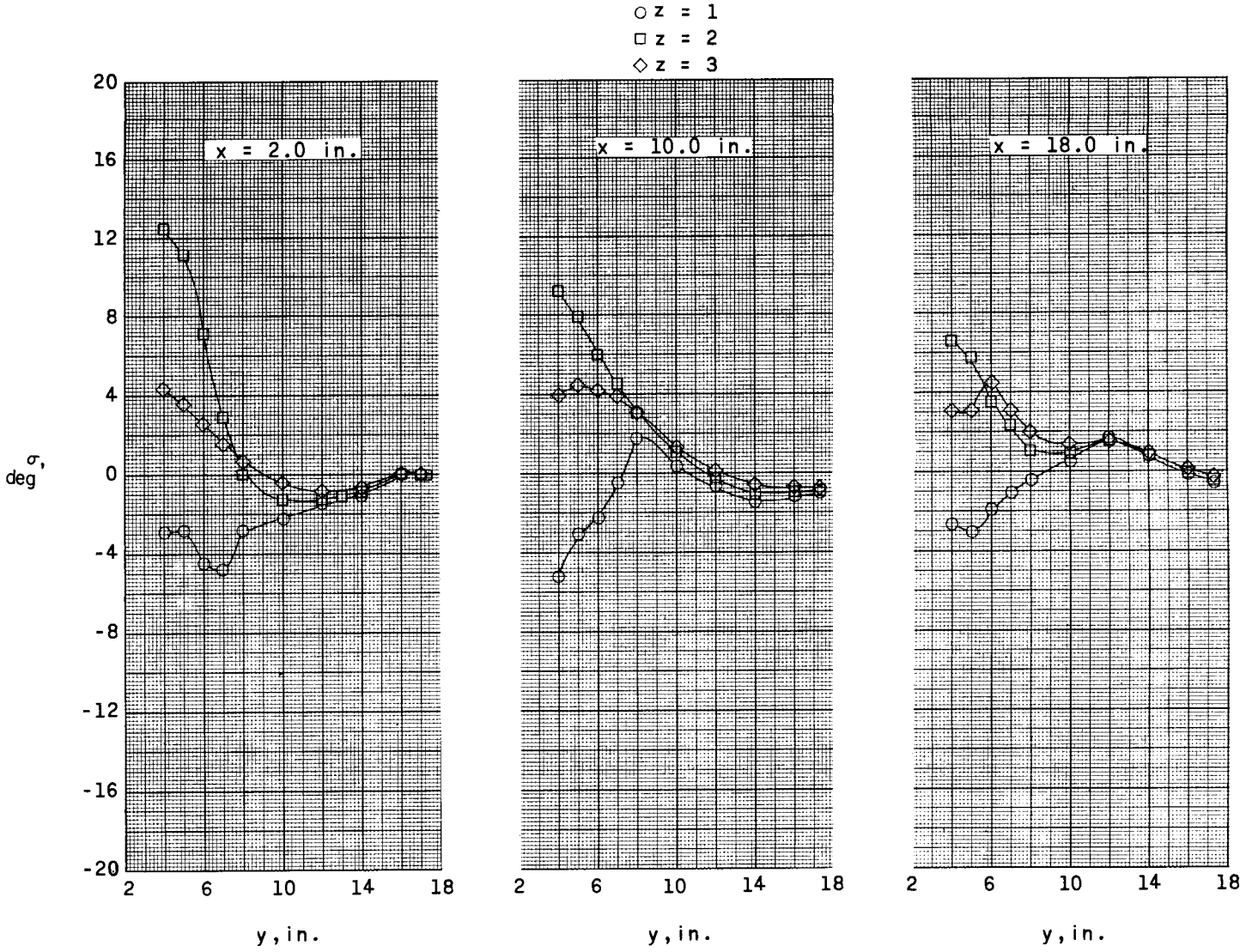

(d) Model B; $\alpha = 0.6^{\circ}$.

Figure 7.- Continued.

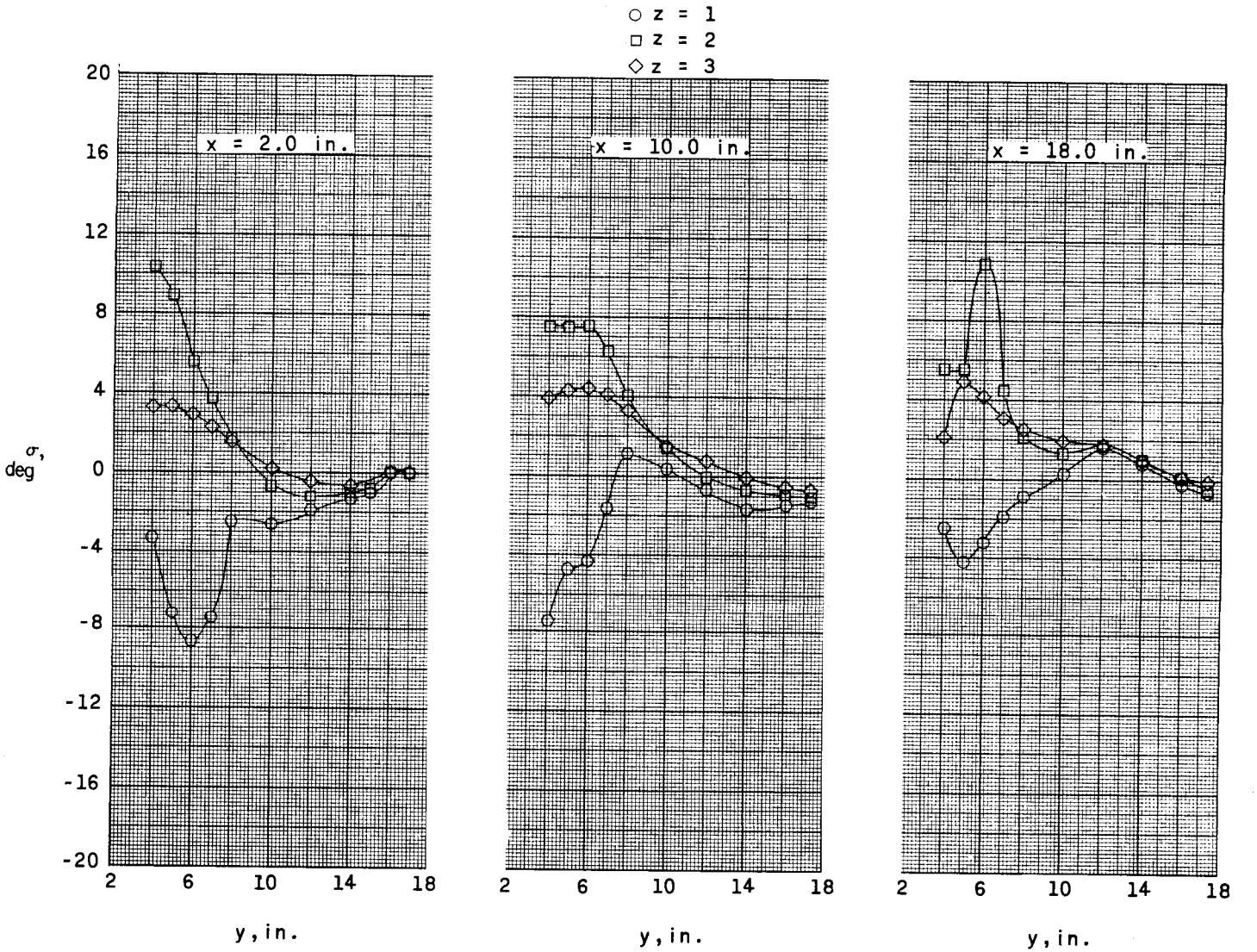

(e) Model B; $\alpha = 2.6^{\circ}$.

Figure 7.- Continued.

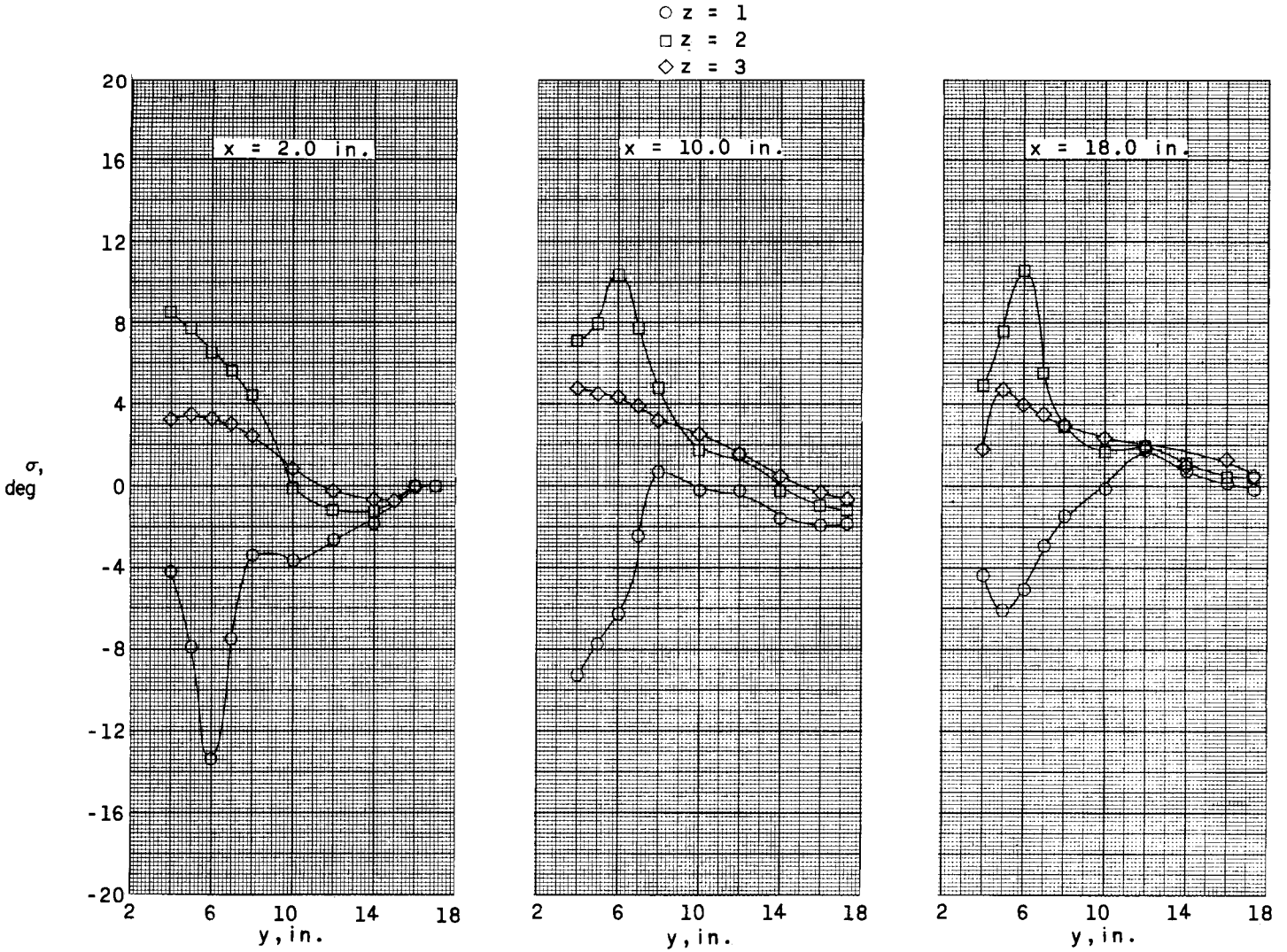

(f) Model B; $\alpha = 4.7^{\circ}$.

Figure 7.- Concluded.